On the origin of the Galactic thin and thick discs, their abundance gradients and the diagnostic potential of their abundance ratios

Nikos Prantzos,[1]⋆ Carlos Abia,[2]⋆ Tianxiang Chen,[1] Patrick de Laverny,[3] Alejandra Recio-Blanco,[3] E. Athanassoula,[4] Lorenzo Roberti ⬤,[5,6] Diego Vescovi,[7,8] Marco Limongi,[9] Alessandro Chieffi[9] and Sergio Cristallo[7,8]

[1]*Institut d'Astrophysique de Paris, CNRS and Sorbonne Université, 98bis Bd. Arago,75014 Paris, France*
[2]*Dpto. Física Teórica y del Cosmos, Universidad de Granada, Avenida de la Fuente Nueva S/N CP:18071 Granada, Spain*
[3]*Université Côte d'Azur, Observatoire de la Côte d'Azur, CNRS, Laboratoire Lagrange, Boulevard de l'Observatoire - CS 34229, 06304 Nice Cedex 4, France*
[4]*Aix Marseille Univ, CNRS, CNES, LAM, 38, rue Frédéric Joliot-Curie 13388 Marseille cedex 13, France*
[5]*Konkoly Observatory, Research Centre for Astronomy and Earth Sciences, Eötvös Loránd Research Network (ELKH), Konkoly Thege Miklós út 15-17, H-1121 Budapest, Hungary*
[6]*CSFK, MTA Centre of Excellence, Konkoly-Thege Miklós út 29-33, Budapest H-1121, Hungary*
[7]*Istituto Nazionale di Astrofisica – Osservatorio Astronomico d'Abruzzo, Via Maggini snc, I-64100 Teramo, Italy*
[8]*INFN - Sezione di Perugia, Via A. Pascoli 23c, 06123 Perugia, Italy*
[9]*Istituto Nazionale di Astrofisica – Osservatorio Astronomico di Roma, Via Frascati, 33, 00078 Monte Porzio Catone, Italy*

ABSTRACT

Using a semi-analytical model of the evolution of the Milky Way, we show how secular evolution can create distinct overdensities in the phase space of various properties (e.g. age versus metallicity or abundance ratios versus age) corresponding to the thin and thick discs. In particular, we show how key properties of the Solar vicinity can be obtained by secular evolution, with no need for external or special events, like galaxy mergers or paucity in star formation. This concerns the long established double-branch behaviour of [alpha/Fe] versus metallicity and the recently found non-monotonic evolution of the stellar abundance gradient, evaluated at the birth radii of stars. We extend the discussion to other abundance ratios and we suggest a classification scheme, based on the nature of the corresponding yields (primary versus secondary or odd elements) and on the lifetimes of their sources (short-lived versus long-lived ones). The latter property is critical in determining the single- or double- branch behaviour of an elementary abundance ratio in the Solar neighbourhood. We underline the high diagnostic potential of this finding, which can help to separate clearly elements with sources evolving on different time-scales and help determining the site of e.g. the r-process(es). We define the 'abundance distance' between the thin and thick disc sequences as an important element for such a separation. We also show how the inside-out evolution of the Milky Way disc leads rather to a single-branch behaviour in other disc regions.

Key words: Galaxy: general – Galaxy: abundances – Galaxy: disc – Galaxy: evolution – Galaxy: formation – Galaxy: Solar neighbourhood.

1 INTRODUCTION

Nowadays there is an exponential increase in the amount of information regarding the stellar populations of our Galaxy. This is due to several large-scale surveys that started during the last decade, like RAVE (Steinmetz et al. 2020), APOGEE (Abdurro'uf et al. 2022), GALAH (Buder et al. 2021), LAMOST (Li et al. 2022), Gaia-ESO (Randich et al. 2022), and last but not least, the results of ESA's Gaia mission (Gaia Collaboration et al. 2022). Those surveys provided information for hundreds of thousands of stars in the 6D space of stellar positions and velocities and in the multidimensional space of elemental abundances, mostly for giants but also for dwarf stars. The determination of another key stellar property, namely stellar ages, still suffers from considerable

uncertainties, but the situation is expected to improve soon due to progress in asteroseismology (as illustrated in e.g. Miglio et al. 2021).

Those observations shed new light on our understanding of the structure of the Milky Way (MW, e.g. Bland-Hawthorn & Gerhard 2016, and references therein). In particular, they have revealed structures in the kinematic and chemical phase space, attributed to debris from old collisions/mergers of various galactic sub-systems with the Galaxy; despite some overlap in their properties, such structures provide important hints on the past history of our Galaxy and the links between its various components (see Helmi 2020, for a recent overview).

Among the main baryonic components of the MW (bulge, bar, stellar halo, and discs), the thick disc remains the most enigmatic. Since its identification as a distinct entity through observations of its vertical density profile (Gilmore & Reid 1983), its various properties have been extensively studied, both locally and across the whole

⋆ E-mail: prantzos@iap.fr (NP); cabia@ugr.es (CA)

Galaxy. It is now clear that it differs from the thin disc in all aspects of its stellar population: spatial, kinematic, metallicity, elemental abundance ratios, and stellar ages. The thick disc is, on average, older than the thin disc (age ∼10 Gy compared to ∼4−5 Gy), less metallic, with a mean [Fe/H][1] ∼ −0.6 dex compared to ∼0 dex, it has higher [α/Fe] at a given metallicity, larger velocity dispersion, and larger scale height. However, in each one of those properties there is an overlap with the thin disc and it is difficult to identify unambiguously the stars of the two discs. As discussed in Kawata & Chiappini (2016), there is no clear definition for the thin and thick discs, even in the case of the MW where ample information is available; the answer depends a lot on how the discs are defined (chemically, kinematically, geometrically, or by age). As a result of this ambiguity, there is still considerable uncertainty on the contribution of the thin and thick discs to the MW mass budget (Anguiano et al. 2020; Everall et al. 2022; Vieira et al. 2022).

An early attempt to model the formation of thick and thin discs of the MW was made by Burkert, Truran & Hensler (1992), who found that it naturally results as a consequence of the gravitational settling and self-regulated chemical and dynamical evolution of an initially hot, gaseous protodisc (top-down formation with high early star formation rate). On the other hand, Quinn, Hernquist & Fullagar (1993), studying *N*-body simulations of halo-disc systems colliding with satellite galaxies found that the kinematical heating induced by such mergers may lead to the formation of thick discs with properties (scale height, vertical velocity distribution, and asymmetric drift) similar to those observed in the MW. Using a semi-analytical, multizone model, Chiappini, Matteucci & Gratton (1997) assumed two periods of star formation, a short and early one (thick disc with high SFR) separated by ∼2 Gy hiatus from a longer one (thin disc with low SFR); their scheme produced a small loop in the [O/Fe] versus [Fe/H] relation at 4 kpc, but did not modify that relation in the outer disc or the Solar neighbourhood. Kroupa (2002b) suggested that the high early SFR (induced by external mergers or perturbations) produced more massive star clusters and high mass stars than the later, low SFR period; the subsequent relaxation of and gas expulsion from those clusters left a characteristic kinematic signature, namely the observed high velocity dispersion of the stars of the thick disc.

Sellwood & Binney (2002) showed that, in the presence of recurring transient spirals, stars in a Galactic disc could undergo important radial displacements. Stars found at corotation with a spiral arm may be scattered to different galactocentric radii (inwards or outwards), a process called *churning* that preserves overall angular momentum distribution and does not contribute to the radial heating of the stellar disc, in contrast to simple epicyclic motion (*blurring*), which does heat the disc radially. Schönrich & Binney (2009) introduced a parametrized prescription of radial migration (distinguishing epicyclic motions from migration due to transient spirals) in a semi-analytical chemical evolution code. They suggested that radial mixing could also explain the formation of the Galaxy's thick disc, by bringing a kinematically 'hot' stellar population from the inner disc to the Solar neighbourhood. That possibility was subsequently investigated with *N*-body models, but controversial results have been obtained. While Roškar et al. (2008) and Loebman et al. (2011) found that secular processes (i.e. radial migration) are sufficient to explain the

kinematic properties of the local thick disc, Minchev et al. (2012) found this mechanism insufficient and suggested that an external agent, like early mergers, is required for that (see also Minchev 2016).

Despite the large number of studies over the years, it still remains unclear the role played by the various processes invoked to explain the morphological, kinematic, and chemical properties of the thick and thin discs of the MW: a clumpy and turbulent early galaxy (e.g. Agertz, Teyssier & Moore 2009; Bournaud, Elmegreen & Martig 2009; Agertz et al. 2021; Beraldo e Silva et al. 2021; Renaud et al. 2021); radial stellar migration, accompanied or not by gas migration (e.g. Schönrich & Binney 2009; Loebman et al. 2011; Kubryk, Prantzos & Athanassoula 2015a; Sharma, Hayden & Bland-Hawthorn 2021b); internal 'heating of the disc' (Kroupa 2002b); various types of mergers, 'dry' or 'wet', minor or major ones, (e.g Villalobos & Helmi 2008; Bekki & Tsujimoto 2011; Navarro et al. 2011; Wilson et al. 2011; Brook et al. 2012; Forbes, Krumholz & Burkert 2012; Bird et al. 2013; Athanassoula et al. 2016; Grand et al. 2018, 2020; Belokurov & Kravtsov 2022); major episodes of infall and/or star formation (Noguchi 2018; Buck 2020; Vincenzo & Kobayashi 2020; Khoperskov et al. 2021; Conroy et al. 2022) or various combinations of the above. For instance, Athanassoula et al. (2016, and in preparation) used high-resolution hydrodynamic *N*-body simulations to follow intermediate, or even major, gas-rich mergers and the corresponding formation and evolution of the thick and thin discs; they found two periods of star formation: an early one, intense and short, and a late one, extended in time but of low amplitude.

On the other hand, using mono-abundance populations (i.e. defined in the plane of [O/Fe] versus [Fe/H]), Bovy et al. (2012) concluded that the thick disc is not really a distinct component of the MW, (see also Rix & Bovy 2013, for a review). The study of Park et al. (2021) with high-resolution cosmological simulations of 19 large-disc galaxies finds that thick and thins discs are commonly formed as 'two parts of a single continuous disc component that evolves with time as a result of the continued star formation of thin disc stars and disc heating'. However, in a recent data analysis of Gaia eDR3 and Lamost (DR7), Xiang & Rix (2022) find distinctive signatures in the MW age−metallicity relation, suggesting that the major merger with Gaia-Enceladus played a significant role in the thick disc formation. It is not clear, however, whether such major events contributed to enhance or rather to inhibit star formation in those early epochs, thus initiating or terminating the thick disc formation (e.g. Ciucă et al. 2023; Conroy et al. 2022). Furthermore, it is not clear whether the formation of the thick disc preceded the one of the thin disc, as commonly assumed, or whether the two were co-eval as suggested in recent studies (Beraldo e Silva et al. 2021; Gent et al. 2022).

The double-branch behaviour of [α/Fe] ratio in the local disc (Fuhrmann 1998; Bensby et al. 2005; Bensby, Feltzing & Oey 2014) attracted a lot of attention, being one of the clearest signatures helping to differentiate observationally the thick from the thin disc (e.g. Adibekyan et al. 2012). This dichotomy has been investigated with both semi-analytical models and chemodynamical ones (with a small fraction of the latter class being referenced in the previous paragraphs). Semi-analytical models can be broadly classified in two categories:

(i) one class of models invokes two periods of star formation in the MW, one corresponding to the thick and one to the thin disc. Those periods are characterized by distinct star formation histories, a shorter early one with intense star formation and a longer late one with a lower star formation, separated by a pause ('hiatus') of several Gy (Grisoni et al. 2017; Noguchi 2018; Lian et al. 2020; Spitoni et al.

---

[1] We adopt here the usual notation [X/H]= log (X/H)$_\star$ − log (X/H)$_\odot$, where (X/H)$_\star$ is the abundance by number of the element X in the corresponding star.

2021). In those models, the double-branch of [α/Fe] versus [Fe/H] is obtained by assuming that at the end of the first phase a strong, metal-poor infall dilutes the gas abundances to considerable amounts (by a factor of 3 at least) and the subsequent star formation creates another [α/Fe] versus [Fe/H] sequence, more or less parallel to the first and starting from lower metallicities and lower [α/Fe] ratios.

(ii) the second class is composed of 'hybrid' models: multizone semi-analytical models of chemical evolution with radial migration introduced in various ways (Schönrich & Binney 2009; Kubryk et al. 2015a; Weinberg et al. 2019, 2022; Johnson et al. 2021; Sharma et al. 2021b); in most cases the dynamics are not treated self-consistently with the chemical evolution and various approximations are made. The two branches of [α/Fe] versus [Fe/H] in the Solar neighbourhood result then from the presence of stars formed not only locally but also in the inner Galaxy, where intense star formation takes place early on. In contrast to the previous case, this is obtained by secular evolution. However, to explain the different dynamics of the thick disc still some different physical processes in the early Galaxy need to be invoked, like e.g. an early highly turbulent or bursty phase, or perturbations by mergers (as in Minchev, Chiappini & Martig 2013; Minchev et al. 2018).

The evolutionary scheme of category (i) seems to be supported by the analysis of Vincenzo et al. (2021), based on the abundances of a sample of red giants from APOGEE DR16. They conclude that the observed bimodality of [α/Fe] versus [Fe/H] probably requires one or more sharp transitions in the disc's gas accretion, star formation, or outflow history in addition to radial mixing of stellar populations. Similarly, Lu et al. (2022a) analyse ∼80 000 sub-giant stars in LAMOST and find a non-monotonic behaviour of the [Fe/H] gradient with age around 8–11 Gy ago. They associate it to the last major merger (Gaia Sausage/Enceladus event) and they claim that this transition plays a major role in shaping the [α/Fe] versus [Fe/H] dichotomy.

The evolutionary scheme of category (ii) is supported by the conclusion of Hayden et al. (2017), based on the orbital and chemical properties of ∼500 stars from the AMBRE survey, that '*the high-[α/Fe] and low-[α/Fe] sequences are most likely a reflection of the chemical enrichment history of the inner and outer disc populations, respectively; radial mixing causes both populations to be observed in situ at the Solar position*'.

In this work, we present a model in line with Hayden et al. (2017), an updated version of the one presented in Kubryk et al. (2015a) (Section 2.1). We present in some detail its main properties in Section 3, showing how secular evolution can create distinct overdensities, corresponding to the thin and thick discs, in the phase space of various properties (e.g. age versus metallicity or abundance ratios versus age). We also show how the non-monotonic behaviour of the stellar [Fe/H] gradient of stars – evaluated at their birth place – with age by Lu et al. (2022a) can be explained by secular evolution and we identify the conditions for that. In Section 4, we focus on the [α/Fe] versus [Fe/H] diagram obtained for the Solar neighbourhood and we show how the double-branch behaviour can also be obtained by secular evolution. Then, in Section 5, we extend the discussion to other abundance ratios and we suggest that in all studies of that kind, the 'distance' in chemical space between thin and thick discs should be quantified in order to clearly identify a single- or double-branch behaviour for a given element. We further suggest a classification scheme of the chemical elements, based on the nature of the corresponding yields (primary versus secondary or odd elements) and on the lifetimes of their sources (short-lived versus long-lived ones). We argue that the latter property is critical in determining the single- or double-branch behaviour of an elementary
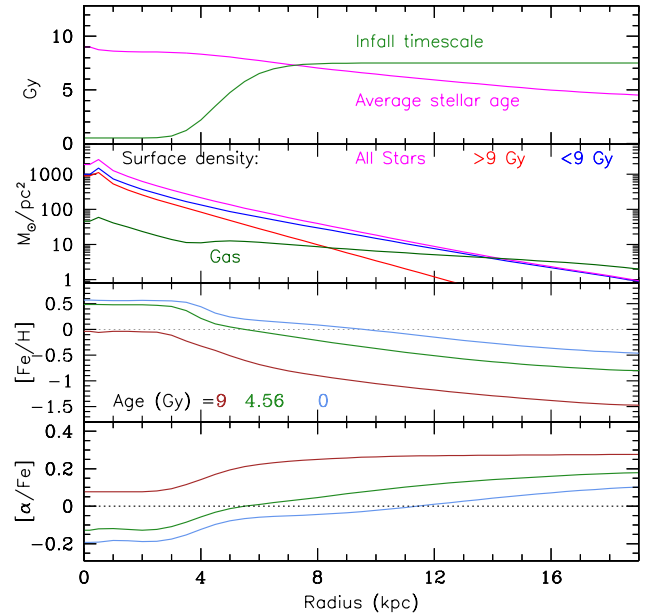

Figure 1. Top panel: adopted infall time-scale (green) and resulting average stellar age (solid magenta) at the end of the simulation. Second panel: final surface density mass profile of gas (green), 'young' stars (age <9 Gy, blue), 'old' stars (age >9 Gy, red), and all stars (magenta). Third panel: Fe abundance profiles in the gas, 9 Gy ago (red), at Sun's formation (4.56 Gy ago, green), and today (blue). Bottom: gaseous [α/Fe] profiles, colour coded as in the previous panel.

abundance ratio in the Solar neighbourhood. We underline the high diagnostic potential of this finding, which can help to separate clearly elements with sources evolving on different time-scales; it would be interesting, in that respect to have a precise evaluation of the abundance distance between the thin and thick disc sequences for the r-elements, which have been suggested to originate either in short-lived sources (collapsars) or long-lived ones (neutron star mergers; e.g. Wanajo, Hirai & Prantzos 2021 and references therein). We also show how the inside-out evolution of the MW disc leads rather to a single-branch behaviour in other disc regions, dominated either by the 'high' [α/Fe] branch (inner disc) or the 'low' [α/Fe] branch (outer disc). In Section 5.3, we discuss other recent studies and we summarize our results in Section 6.

2 THE MODEL

2.1 Model

We summarize here the main features of the Kubryk et al. (2015a) model and the new ingredients adopted in this work.

2.1.1 Stars and gas

The Galactic disc is gradually built up by infall of primordial gas in the potential well of a dark matter halo with mass of 10^{12} M$_\odot$, the evolution of which – mass growing with time – is obtained from numerical simulations (from Li et al. 2007). The one-dimensional (1D) disc is built 'inside-out' through infall of gas of primordial composition. The infall time-scales are fairly short (0.5 Gy) in the inner regions and increase progressively outwards, reaching 7.5 Gy at 8 kpc and staying nearly constant after that (see top panel in Fig. 1). The star formation rate depends on the local surface density

of molecular gas Σ_{H_2}, the latter being calculated from the total gas through the prescription of Blitz & Rosolowsky (2006).

The disc is split in concentric annuli of radial width $\Delta R = 0.5$ kpc, interacting through radial motions of their stars. Stars move radially from their birthplace due to epicyclic motions around their guiding radius (blurring) and to changes of their guiding radius (churning), as explained below. The innovative aspect of the model is that it accounts for the fact that radial migration moves around not only 'passive tracers' of chemical evolution (i.e. long-lived low-mass stars, keeping in their photospheres the chemical composition of the gas at the time and place of their birth), but also 'active agents' of chemical evolution, i. e. long-lived nucleosynthesis sources (such as SNIa producing Fe and low mass stars producing s-process elements), which may release their products away from their birth place. The probabilistic formalism for radial migration takes into account the finite lifetime of stars (see Kubryk et al. 2015a). In practice, stars more massive than 4 M$_\odot$ (with lifetimes <0.3 Gy), do not live long enough to participate in such motions and die in their birth zone (here taken to be 0.5 kpc wide). This also applies to giant molecular clouds, their lifetime being comparable to those of massive stars, of the order of $10-30$ Ma (Jeffreson et al. 2021).

In the Kubryk et al. (2015a, b) model, the thick disc is assumed to be the oldest part of the Galactic disc, older than ~ 9 Gy (see Binney & Sanders 2014), while the thin disc is younger than 9 Gy. In this work, the thin and thick discs appear naturally as overdensities in the phase space of various properties of stars in the Solar neighbourhood (age, metallicity, and abundance ratios) as we discuss in the next sections, and they do not result from a pause in star formation. Instead, they are produced in a continuous inside-out formation process, as suggested by the recent simulations of Park et al. (2021). These simulations have unprecedentedly high spatial resolution (aimed to reach $\Delta x \sim$ 34 pc at redshift $z = 0$), making them ideal to investigate the detailed structures of galaxies. Park et al. (2021) find that spatially defined thin and thick discs are not entirely distinct components in terms of formation process, but rather two parts of a single continuous disc component that evolves with time as a result of the continued star formation of thin-disc stars and disc heating.

The radial displacements of stars due to blurring and churning are calculated statistically, with prescriptions adopted on the basis of N-body SPH simulations (Kubryk, Prantzos & Athanassoula 2013, 2015a). Blurring is calculated by using the stellar radial velocity dispersion, which is assumed to evolve with time as $\sigma_r \propto \tau^\beta$, but in contrast to Kubryk et al. (2015a) where $\beta = 0.33$, here we adopt $\beta = 0.25$, based on analysis of numerical simulations of the heating of MW-type discs by Aumer, Binney & Schönrich (2016) and of MW observations from GALAH, LAMOST, APOGEE, the NASA Kepler and K2 missions, and Gaia DR2 from Sharma et al. (2021a). We assume that the old disc (age >9 Gy today) inherited a large radial velocity dispersion of $\sigma_r(R) = 50 e^{-(R-8)/11}$ km s^{-1}, where R is the radius in kpc and 11 kpc is the characteristic scale of the decline of radial dispersion of the thick disc (see Bland-Hawthorn & Gerhard 2016, and references therein[2]). Such a high dispersion can be acquired either during an initial, highly turbulent phase of the gas (e.g. Bournaud et al. 2009; Brucy et al. 2020), through a major merger around 8–9 Gy ago, like Gaia-Enceladus (Helmi 2020, and references therein), or through some combination of various physical processes.

Indeed, the recent analysis by Yan et al. (2019) of a sample of 307 246 A, F, G, K-type giant stars from the LAMOST spectroscopic survey and Gaia DR2 survey concludes that the formation of the thick disc could be affected by more than one process: the accretion model seems to have played a prominent role, but other formation mechanisms, such as radial migration or disc heating could also have a contribution. Also, Beraldo e Silva et al. (2021), analysing the kinematics and orbits of 23 795 turnoff and giant stars with 6-D phase-space coordinates from Gaia-DR2 find that in the Solar neighbourhood, about half of the old thin disc stars can be classified as migrators, while for the thick disc this migrating fraction could be as high as $\sim 1/3$.

2.1.2 Nucleosynthesis sources

The Kubryk et al. (2015a, b) version of the model uses the metallicity-dependent yields of Nomoto, Kobayashi & Tominaga (2013) for massive stars with no mass loss, and Karakas (2010) for low and intermediate masses (LIMS), which are calculated up to a metallicity of $Z = 2 Z_\odot$, and are appropriate for the study of the inner Galactic disc. However, in Karakas (2010) the s-process is not considered. Prantzos et al. (2018, 2020) adopted for LIMS the yields of Cristallo et al. (2015), which include the s-process and are calculated up to $Z = 2 \times 10^{-2} \sim 1.45 Z_\odot$, and for massive stars those of Limongi & Chieffi (2018), which include the effect of mass loss and stellar rotation but go only up to $Z_\odot$. Here, we use the same yields augmented by a new set of models at $Z = 3 \times 10^{-2} \sim 2 Z_\odot$, calculated for this study by the same authors and available in the corresponding data bases;[3] indeed, the study of the inner disc, which may reach metallicities as high as 2–3 $Z_\odot$, requires the use of model yields from superSolar metallicity stars. Also, in contrast to all previous studies of radial migration plus chemical evolution in the Galactic disc, this is the first study using stellar yields from massive stars dependent on rotational velocity. The IDROV (Initial Distribution of ROtational Velocities) is presented in Prantzos et al. (2018) for a 1-zone model, where it was 'calibrated' as function of metallicity in order to reproduce key observables and it is also adopted here. We note that a comparative study of Philcox, Rybizki & Gutcke (2018) found that the yields and IDROV adopted in Prantzos et al. (2018) reproduce best the proto-solar abundances – compared to other sets of yields – for a large number of elements.

The initial mass function (IMF) of Kroupa (2002a) with a slope 1.3 for the high masses, is considered. A phenomenological rate of SNIa is adopted, based on observations of extragalactic SNIa Maoz & Graur (2017) while their metallicity-dependent yields are from Iwamoto et al. (1999). In order to calculate the rate of ejecta (both for stars and SNIa) as a function of time, the formalism of single particle population is used because it can account for the radial displacements of nucleosynthesis sources and in particular of SNIa, as discussed in Appendix C in Kubryk et al. (2015a).

3 GALACTIC DISC PROPERTIES OF THE MODEL

3.1 Overall properties

Some key features of the model, relevant to our discussion, are displayed in Fig. 1. The inner regions (here taken to be as those with Galactocentric distance $R_G < 4$ kpc) are formed quite rapidly,

---

[2]See Mackereth et al. (2019) for a more detailed analysis of velocity dispersions of the MW.

[3]http://fruity.oa-abruzzo.inaf.it and http://orfeo.iaps.inaf.it/index.html for LIMS and massive stars; respectively.

since the adopted characteristic time-scale of gas infall is of the order of ~1 Gy (upper panel), while intermediate regions (4 < R_G < 10 kpc) formed within a few Gy and the outer regions after several Gy. As a result, the average age of stars today is ~9 Gy for the inner disc, 6–8 Gy for the intermediate disc, and <5 Gy for the outer disc.

The final stellar surface density profiles, at T = 12 Gy (second from top panel in Fig. 1) are quasi-exponential, with characteristic scale lengths of R_T ~ 1.9 kpc for the old disc (age >9 Gy), ~2.8 kpc for the young disc (<9 Gy), and 2.6 kpc for the total disc. These values should be compared to Bland-Hawthorn & Gerhard (2016), who suggest $R_T = 2.0 \pm 0.2$ kpc for the thick disc and $R_T = 2.6 \pm 0.5$ kpc for the thin disc, which are, however, defined chemically in their case. The resulting present day gas surface density profile is essentially flat, going through a broad maximum at R_G < 5 kpc, and slowly declining outwards, again in fair agreement with observations (see e.g. Appendix A in Kubryk et al. 2015a).

The Fe abundance profiles in the gas (third panel from the top in Fig. 1) are displayed for ages 0 (today), 4.56 Gy (Sun's formation), and 9 Gy. They are exponentially decreasing with galactocentric distance at all ages. The abundance gradient is getting smaller (in absolute value) with time, as a consequence of the adopted inside-out star formation scheme. The present day gradient is d[Fe/H]/dR ~−0.06 dex/kpc in the range 4 < R < 12 kpc, again in fair agreement with observed values (e.g. Minniti et al. 2020; Spina, Magrini & Cunha 2022, and references therein). It is approximately zero in the innermost regions, where the gas fraction is extremely small and chemical evolution has reached a steady state: metal-poor gas returned from old low-mass stars dilutes the fresh metal content released by the few young massive stars. We note the flat metallicity profile in the inner 3–4 kpc of the disc at early times (the 9 Gy curve) due to the short infall time-scale assumed for those regions and the resulting uniformly high SFR; this is in agreement with the recent finding of Xiang & Rix (2022) that the star forming gas in the old disc of the MW had small metallicity variations (less than 0.2 dex), otherwise the resulting [Fe/H]–age relation would display larger scatter than what they infer from their data analysis of Gaia eDR3 and LAMOST DR7 surveys.

Finally, the bottom panel of Fig. 1 displays the [α/Fe] profiles, decreasing inwards, again as a consequence of inside-out star formation: SNIa, which are the main Fe source, enrich the inner regions with Fe for a larger fraction of the time than the outer ones, which form their stars later. Thus, their time-integrated Fe ejecta per unit mass of gas processed is higher in the inner Galaxy and the [α/Fe] ratio is lower there.

Fig. 2 displays some of the properties of the model and their consequences for the final stellar distributions as function of Galactocentric radius. In the top panel is displayed the evolution of the adopted profiles of radial dispersion of stars as function of time. For the first 3 Gy of Galactic evolution (the thick disc), stars are assumed to be born with a time-independent radial velocity dispersion $\sigma_r(R) = 50e^{-(R-8)/11}$ km s^{-1} (see Section 2.1.1), here shown by a red dashed curve. For the subsequent 9 Gy (the thin disc), stars are assumed to inherit at their birth the velocity dispersion of the 'settled' gas (flat profile at $\sigma_r(R) = 10$ km s^{-1}, corresponding to the gas dispersion today), then σ_r increases proportionally to $\tau^{0.25}$, as shown here for times $\tau = 3, 6$, and 9 Gy after stellar birth; the latter curve corresponds to the present-day $\sigma_r(R)$ profile of the MW disc.

The two other panels of Fig. 2 indicate the fraction of stars present today in the annuli centered at Galactocentric radii R = 3, 8, and 13 kpc (blue, red, and green histograms, respectively) as a function of the corresponding birth radii. For the 'old' stars (>9 Gy),
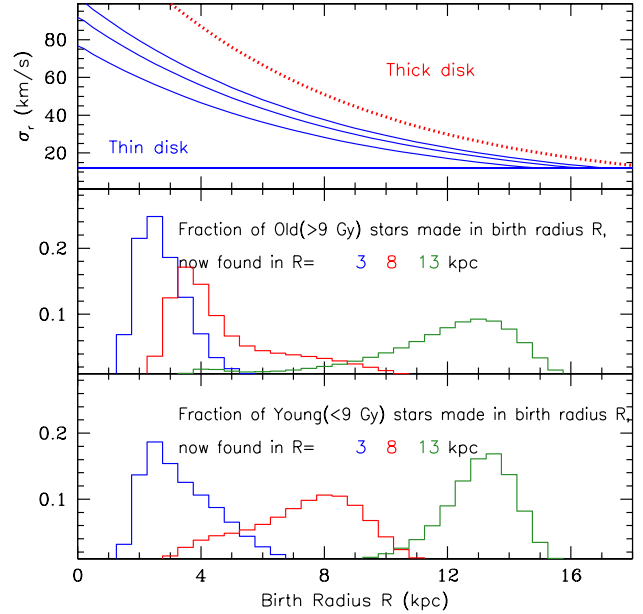

Figure 2. Top: radial velocity dispersion σ_r of stellar populations in the thin disc (blue curves), after 0, 3, 6, and 9 Gy (from bottom to top); the lowest curve corresponds to the velocity dispersion of the gas. The stars of the thick disc are assumed to be formed in the first 3 Gy with a velocity dispersion indicated by the red dotted curve (see text). Middle: fraction of 'old' stars born in radius R now found in three characteristic radii $R_G = 3, 8$, and 13 kpc (blue, red, and green histograms, respectively). Bottom: same as in previous panel, for 'young' stars (age <9 Gy).

here qualified as the thick disc (middle panel), the largest fraction originates in the inner disc (2–4 kpc) where most stars are formed quite early; at such early times, there are very few stars formed outside 4–5 kpc, as can be seen from the adopted infall time-scales in the top panel of Fig. 1. Of particular importance is the resulting distribution for the stars in the Solar neighbourhood (red histogram in the middle panel of Fig. 2): an increasingly large fraction comes from the inner disc and ~ 15 per cent–20 per cent of all local old stars are formed at R_G ~3–4 kpc. This is in excellent agreement, both qualitatively and quantitatively, with the findings of Minchev et al. (2013, their fig. 3, left-hand panel) or Sharma et al. (2021a, their fig. 10, 3d column), where they display the fractional contribution of various birth radii to the Solar neighbourhood population of stars older than 10 Gy. In contrast, the outer disc receives only a small contribution of its old stars from the inner disc (green histogram in the middle panel).

On the other hand, most of the 'young' stars (<9 Gy, thin disc, bottom panel in Fig. 2) are formed close to their present position, but they may receive substantial contributions from regions further away, mostly from the inner disc. This is particularly true for the Solar neighbourhood in a Galactocentric distance of R =8 kpc (red histogram), which receives a contribution from stars born at R_{birth} = 3 kpc. As noticed long ago (e.g. Chiappini 2009; Minchev et al. 2013, and so on), this contribution from the inner disc explains the existence of superSolar metallicity stars in the Solar neighbourhood today (see next sub-sections).

The results regarding the radial displacement of the disc stars of our model are summarized in Fig. 3, displaying the distribution of birth radii versus final radii for all the star particles of the simulation. Outside $R_G = 3$ kpc, the average birth radius of 'young' stars (blue curve) is found to be up to ~2 kpc inwards of their
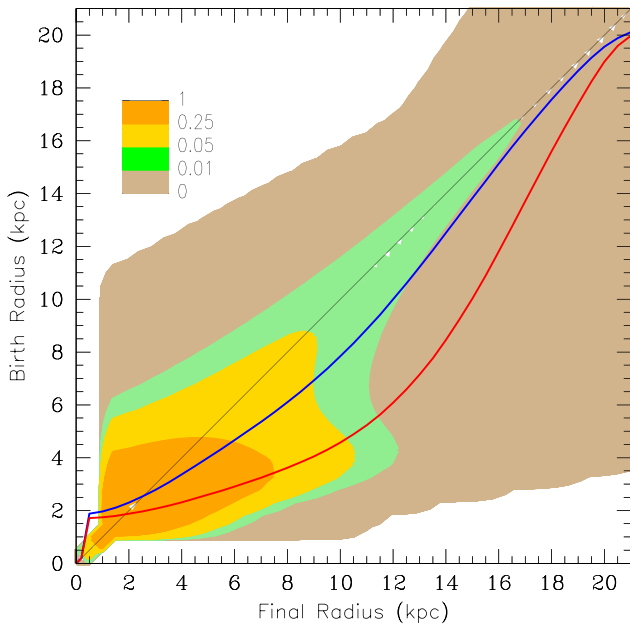
Figure 3. Isocontours of star numbers ($N_{\max} = 1$) in the plane of birth radius versus final radius at the end of the simulation (T = 12 Gy). The average birth radius of stars at each final radius is indicated by the blue curve for the 'young' disc (age <9 Gy) and by the red curve for the 'old' disc (age >9 Gy). In the insert box are depicted the isocontour levels, also adopted in all subsequent figures (unless otherwise stated).

present day position. In particular, the average birth radius of Solar neighbourhood stars is at $R_G = 6$ kpc, again in agreement with e.g. Minchev et al. (2013) or Kubryk et al. (2015a). For 'old' stars, the average birth radius (red curve) is found further inwards, as discussed in the previous paragraph. As found in Beraldo e Silva et al. (2021), stars can visit the Solar Neighbourhood by oscillating around their guiding radius (blurring, most relevant for eccentric orbits) or via radial migration (churning).

Feltzing, Bowers & Agertz (2020) performed a bold and thorough investigation of the amount of radial migration in the MW disc, using data for red giant branch stars from APOGEE DR14, parallaxes from Gaia, and stellar ages based on the C and N abundances. In order to estimate the birth radii of the stars, they used results of the ISM abundances in various epochs, as obtained in the models of Minchev et al. (2018), Frankel et al. (2018), Sanders & Binney (2015), and Kubryk et al. (2015a). They evaluated the fractions of stars that moved radially, either through blurring or churning and found that half of the stars have experienced some sort of radial migration, 10 per cent likely have suffered only from churning, and a modest 5 per cent–7 per cent have never experienced either churning or blurring. They found that their results depend little on the radial abundance profiles of the adopted models, despite the differences among the latter. They also found that the Sun likely formed between 5.5 and 7 kpc from the Galactic centre in all the aforementioned simulations, again in agreement with our results in the previous paragraph; see, however, next sub-section for a smaller Solar R_B invoked by Lu et al. (2022a).

3.2 Age versus metallicity in the local disc

Fig. 4 displays the evolution of [Fe/H]. The upper panel shows the evolution in the gas of all the radial zones of the simulation. The zones are colour-coded according to their position: red (inner disc,
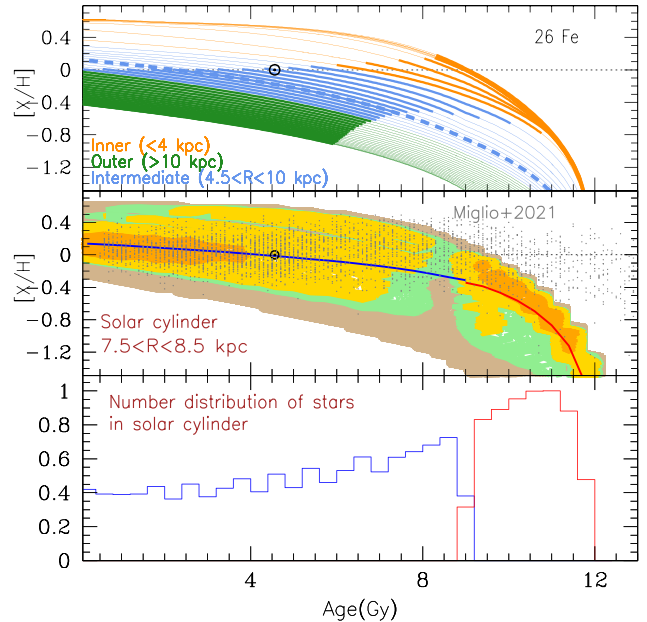

Figure 4. [Fe/H] versus age. Top: evolution of [Fe/H] in the gas in each radial zone. Inner disc ones ($R < 4$ kpc) are in red, outer disc ones ($R > 10$ kpc) in green, and intermediate ones in blue; the dotted curve corresponds to $R_\odot = 8$ kpc. The *thick* portions of each curve correspond to a local star formation rate higher than the average one for that zone (see text). Middle: [Fe/H] of stars present in the Solar cylinder [$7.5 < R$ (kpc) <8.5] at the end of the simulation. Isocontours correspond to star number counts (colour coded as in Fig. 3), while the blue and red curves indicate the average [Fe/H] for 'young' and 'old' stars, respectively, and data from Miglio et al. (2021) are displayed as grey points (see text). Bottom: number distribution of stars present today in the 'Solar cylinder'.

with same short infall time-scales of ∼1 Gy), green (outer disc, same large infall time-scales of ∼8 Gy), and blue (intermediate disc, with widely varying infall time-scales). The corresponding star formation activity in the various zones is depicted by the thick portions of the curves, denoting star formation rates higher than the average of each zone. For the inner zones, that period occurs early on (in the first ∼4 Gy), while for the outer zones star formation activity is strongest in the last 5−6 Gy and an intermediate situation holds for the intermediate (blue) zones. In all the cases, the star formation activity is never high at superSolar metallicities, which suggests a rather small fraction of Galactic stars with such metallicities.

Solar metallicity is reached only fairly recently in the gas of the Solar neighbourhood in our model. This is in agreement with observations of local gas, showing that the abundances of several elements within ∼1 kpc from the Sun are Solar to within ±0.04 dex (Cartledge et al. 2006). It is also in agreement with observations of young B-stars both in the field and in the nearby star forming region of Orion (Nieva & Przybilla 2012), displaying Solar abundances. The straightforward implication of those observations is that, either (i) the Sun was formed in its current Galactocentric radius of $R_G = 8$ kpc and the local gas metallicity has varied very little since then, or (ii) the Sun was formed in the inner disc, a couple of kpc inwards from its inner position. The former option implies that, for about half the age of the thin disc, there is an implausibly perfect equilibrium between metal enrichment of the gas from various nucleosynthesis sources (even those evolving on different time-scales, like α-elements from massive stars and Fe from SNIa) and metal dilution (from ejecta of metal poor old low-mass stars or late infall). Option (ii) implies

that the Sun migrated to its present-day position from its birth place, located a couple of kpc inwards in the disc (e.g. Nieva & Przybilla 2012; Minchev et al. 2013; Kubryk et al. 2015a). This is what we found also here: [Fe/H] becomes zero 4.56 Gy ago in the gas of the zone at Galactocentric radius $R_G \sim 6$ kpc.

The middle panel of Fig. 4 shows the situation for the stars now present in the 'Solar neighbourhood', taken as an annulus of width $\Delta R = 1$ kpc centered at Galactocentric radius $R_0 = 8$ kpc. We also display the data of Miglio et al. (2021), showing a disagreement with the model for the oldest ages, which is explainable by the still important uncertainties (of ± 20 per cent at least) currently affecting the evaluation of stellar ages. The coloured iso-density contours of the model show two regions of enhanced stellar populations: an early one in the first ~ 3 Gy with rapidly increasing [Fe/H] and a late one, extended over the past ~ 7 Gy with very slowly increasing [Fe/H]. Comparison to the upper panel suggests that the early enhancement results from stars formed mainly in the inner disc in the first ~ 3 Gy and brought in the Solar neighbourhood due to the assumed high radial velocity dispersion at early epochs. The late enhancement of stellar population with [Fe/H]~ 0 dex corresponds to stars formed at late times mostly locally, i.e. in the 7–9 kpc region.[4]

The gap between the two densely populated regions, namely the paucity of stars around 8–9 Gy is due to the combination of two factors: (i) our assumption of a very rapid and efficient early star formation in the inner disc (due to the very short infall time-scale of ~ 1 Gy for $R_G < 4$ kpc), while at larger radii stars are formed at a slower rate; and (ii) the assumption of a highly turbulent gaseous disc in the first 3 Gy, which makes possible the presence of a large number of old stars from the inner disc at 8 kpc. Stars from intermediate regions (4–8 kpc) are also present in the Solar neighbourhood now, but they have been formed with largely different star formation efficiencies and their [Fe/H] distribution (characterizing the metallicity dispersion at a given age) is fairly wide at ages 8–9 Gy; it becomes less wide at younger ages, because younger stars have less time to migrate up to the Solar vicinity. In summary, the Solar neighbourhood is found to be less densely populated with stars 8–9 Gy old, an age which marks the change in the regime of both radial displacement and time-scale of star formation.

We note that similar well-defined overdensities in the age-metallicity plane are found in the recent analysis of $\sim 250\,000$ sub-giant stars from LAMOST DR7 spectroscopic survey and Gaia EDR3 mission by Xiang & Rix (2022). The two overdensities are separated by a gap at age 8–9 Gy, as in our case. However, the ages of the oldest stars in Xiang & Rix (2022) extend up to 15 Gy (instead to 12 Gy in our case), making the duration of the thick disc phase much longer than usually assumed.

Those two enhancements of the stellar density in the age–metallicity plane, are reproduced also in the phase-space of other observables, like the abundance metallicity ratios, as we shall see in subsequent sections. This concerns in particular the [α/Fe] versus [Fe/H] relation and the chemical differentiation of the thin and thick discs.

In the bottom panel of the same figure, we display the number distribution of stars present today in the Solar neighbourhood. Since

---

[4]We note that both the middle and bottom panels concern the stars that are alive today and not all the stars ever formed. This means that their numbers depend on the SFR of the various radial zones, but for older ages, the upper part of the IMF is missing; e.g. for an 11-Gy-old population, only stars below 0.9 $M_\odot$ currently remain, i.e. ~ 30 per cent of the initial mass of stars formed in that period and 10 per cent of the initial number are missing.
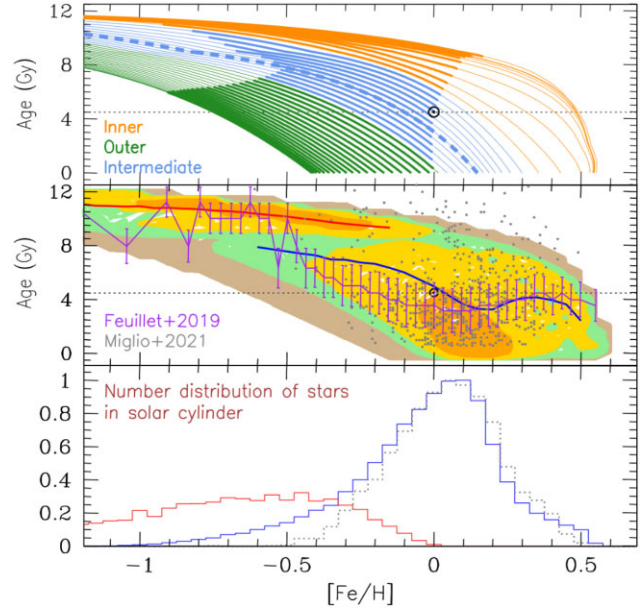
Figure 5. Age versus metallicity. Top: relation for the radial zones of the model, colour code as in Fig. 4. Middle: isodensity contours in the age versus [Fe/H] plane in the Solar cylinder, colour coded as in Fig. 3, while the blue and red curves indicate the average [Fe/H] for 'young' and 'old' stars, respectively; they are compared to observational data from Feuillet et al. (2019, violet curve,vertical bars) and Miglio et al. (2021, grey points). Bottom: metallicity distributions for Solar neighbourhood for thick (red) and thin (blue) discs; the latter is compared to red giant data from Miglio et al. (2021, grey dotted histogram).

our model is a 1D and assumes azimuthal symmetry (no vertical dimension), it is more appropriate to refer to this region as 'Solar cylinder'. We emphasize that this distribution is not representative of the local star formation rate, since the fraction of migrated stars increases with age; this concerns stars born elsewhere that migrated to the Solar cylinder, as well as stars formed locally that have migrated to other zones.

Fig. 5 displays another important feature of disc models with radial migration. The previous relation is now shown as age versus metallicity. In the middle panel, the model results show again the double-branch behaviour already discussed in the previous paragraphs. The results are compared to those of Feuillet et al. (2019), who used a sample of 81 000 stars from SDSS and APOGEE data with Gaia DR2 parallax measurements to derive the age–metallicity relation in several regions of the Galactic disc; their study covered the inner, local and outer disc, as well as the regions near the plane and away from it. The results shown are those for $7 < R(\text{kpc}) < 9$ and $0 < z(\text{kpc}) < 0.5$ in fig. 3 of Feuillet et al. (2019) (shown with vertical bars and corresponding average values in our Fig. 5).

At low metallicities ([Fe/H] < -0.5) the data suggest a plateau for old ages, which corresponds well to the flat shape of the upper overdensity of our model; these are obviously stars of the 'old' (= thick) disc. At higher metallicities, the average age of the observations declines slowly with increasing metallicity, reaching a value of ~ 3 Gy at [Fe/H]~ 0, above which it increases again and reaches a plateau around 4 Gy at [Fe/H]~ 0.5. As noticed in Feuillet et al. (2019), the age upturn at $\sim$Solar metallicity was predicted by the model of Kubryk et al. (2015a) and it is a clear sign of radial migration. While young stars with [Fe/H]~ 0 are formed in the Solar ring (and adjacent regions), higher metallicity stars are formed in

the inner disc and transported in our vicinity by radial migration (see upper panel). As discussed in Kubryk et al. (2013), this process proceeds at an average speed of $v_r \sim 1$ kpc Gy^{-1} in the radial direction. Stars with superSolar metallicities have been formed at Galactocentric radii of 3–6 kpc and have travelled to our vicinity on time-scale of $\sim \Delta R / v_r \sim 4-5$ Gy. Our results in this work reproduce quite well the observations (the decline and rise of the average age as function of metallicity) although the model average age is by ~ 1 Gy older. A further sign of downturn is observed in the data as well as in our model around [Fe/H] = 0.3–0.4 dex. Feuillet et al. (2019) argue that this feature represents the few most metal-rich stars that were formed rather recently in the innermost disc ($R < 2-3$ kpc) and had time to migrate to the Solar neighbourhood. Our results (upper and middle panel in Fig. 5) confirm their conclusion.

Similar results are obtained in the recent study of Johnson et al. (2021) who use a 'hybrid' model: radial migration with positions and kinematics of star particles is taken from a N-body + SPH code, as in Minchev et al. (2013), and different star formation histories are explored. As in Kubryk et al. (2015a), the stars may release their nucleosynthesis products away from their birthplace.[5] Johnson et al. (2021) obtain a similar age versus metallicity relation (see their fig. 16 bottom) to the one displayed in our Fig. 5 (middle): slightly larger average ages than the observations of Feuillet et al. (2019) at sub-Solar and superSolar metallicities and approximately the same average age as in Feuillet et al. (2019) at Solar metallicity; most importantly, the U-turn shape around $Z_\odot$ (indicative of radial migration as discussed in the previous paragraph) accompanied by a downturn at the highest metallicities. Despite the very different assumptions of the two models, the similarity of the results between the two studies and the observations suggest that the adopted inside-out scheme of star formation, accompanied by radial migration, provides a rather realistic description of the evolution of the thin disc.

In a recent work, Dantas et al. (2022) report the identification of a set of old super metal-rich ($+0.15 \leq$ [Fe/H] $\leq +0.50$) dwarf stars with low eccentricity orbits that reach a maximum height from the Galactic plane between 0.5 and 1.5 kpc and have median ages 7–9 Gy. They suggest that most stars in this population originated in the inner regions of the Milky Way (inner disc and/or bulge) and later migrated to the Solar neighbourhood, mostly through churning. An inspection of our Fig. 5 shows that, in our model, such stars would be formed in Galactocentric distances around 2–3 kpc during the transition phase from thick to thin disc. They are considerably older (by several Gy) than most stars of similar metallicities currently present in the Solar neighbourhood. The detailed analysis of their abundance patterns, which are presented in Dantas et al. (2022), would provide further insight into the nucleosynthesis in those remote Galactic regions and will be the topic of future work.

In the lower panel of Fig. 5 we display the metallicity distribution of stars for the thin and thick discs in the local cylinder. We compare the one for our thin disc (all stars with ages <9 Gy) with data for the thin disc obtained recently by Miglio et al. (2021) for 3300 giant stars with available Kepler light curves and APOGEE spectra. In that study, stellar masses and ages are obtained from a combination of seismic indices and photospheric constraints, and the authors emphasize that those properties depend on the observational constraints via power laws, which lead to '*a blurred view at older stellar ages*'. For that reason, and because that survey obtains quite old ages (up to 14 Gy), which are substantially higher than the 12
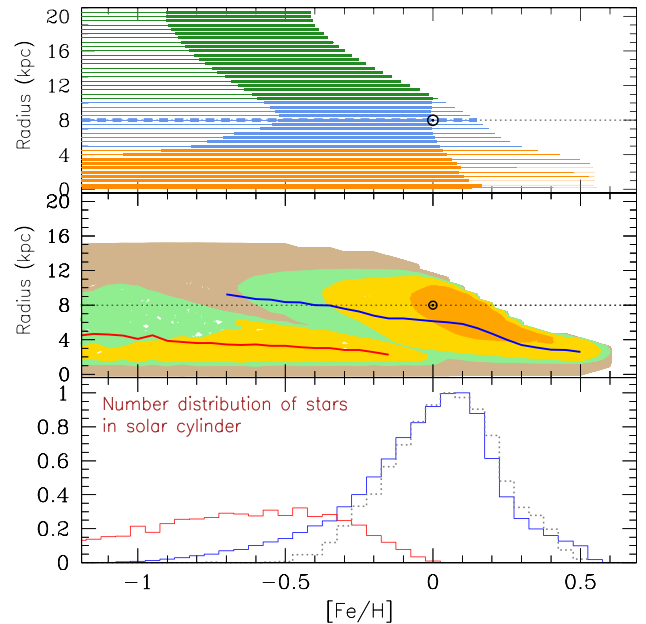

Figure 6. Birth radius versus stellar metallicity. Top: evolution of gaseous [Fe/H] in all the radial zones of the model, with colour coding as in Fig. 4. Middle: isodensity contours for the birth radii of stars present today in the Solar cylinder, colour coded as in Fig. 3, while the blue and red curves indicate the average [Fe/H] for 'young' and 'old' stars, respectively; the thick solid curves indicate averages at a given metallicity for the old (>9 Gy, red) and young (<9 Gy, blue) discs. Bottom: metallicity distributions for Solar neighbourhood for thick (red) and thin (blue) discs; the latter are compared to red giant data from Miglio et al. (2021, grey dotted histogram).

Gy of our oldest stars, we chose to compare our results only with the thin disc data of Miglio et al. (2021), which we consider to correspond to stellar age <9Gy (in agreement with our definition). In the bottom panel of Fig. 5 we find a fairly good agreement in most of the metallicity range between model and data, except in the lowest metallicities where our model displays a rather extended tail down to [Fe/H] ~ -1, while the Miglio et al. (2021) thin disc does not go below [Fe/H] ~ -0.5.

Fig. 6 illustrates clearly the spatial origin of the stars present today in the Solar neighbourhood for the various metallicity ranges. The star formation activity throughout the disc has been more intense at sub-Solar metallicities (top panel), although this occurred at fairly early times in the inner zones and at late times for the outer zones, as discussed in previous paragraphs. The bulk of the stars in the Solar cylinder is around [Fe/H]~ 0 and originates from the $5-9$ kpc region. The high metallicity tail of the distribution of stars younger than 9 Gy (blue histogram in lower panel) originates from zones at the interior of 4 kpc, and on average in the zone at $R = 3$ kpc (blue curve in middle panel). The low metallicity tail of the young (= thin) disc has an important contribution from the outer zones at $9-10$ kpc, as already suggested in Haywood (2008) and Schönrich & Binney (2009), on the basis of observational and theoretical analysis, respectively. The old (= thick) disc extends up to quasi-Solar values and its stars originate mostly from radii <6 kpc as already illustrated in Figs 2 and 3. This is also valid for the superSolar metallicity stars of the thin disc, as already discussed in the previous paragraphs and in Dantas et al. (2022).

---

[5]This is an important implication of radial migration for long-lived nucleosynthesis sources, as first pointed out in Kubryk et al. (2013).
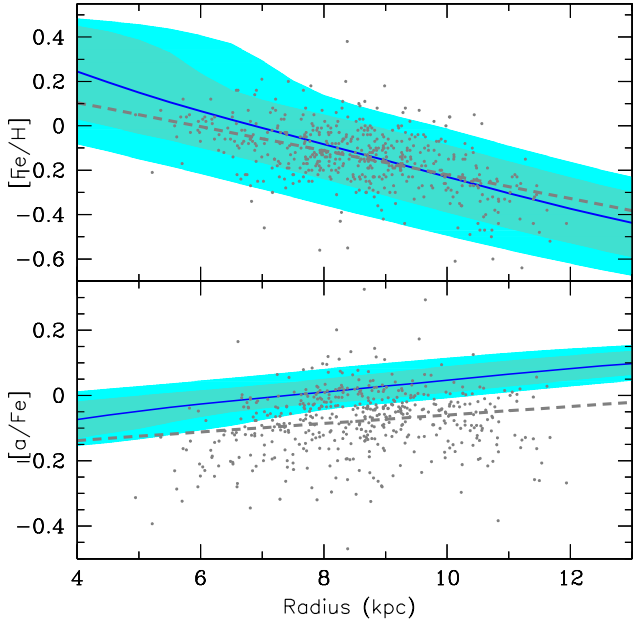
Figure 7. Top: metallicity profile of open clusters (ages in the 0–6 Gy range) as observed by Gaia DR3 (Gaia Collaboration et al. 2022), with the average value indicated by the grey dashed curve; they are compared to model results (blue curves), with the shaded areas indicating the 1-sigma and 2-sigma density contours. Bottom: same as in previous panel, for the [α/Fe] profile.

3.3 Abundance profiles and their evolution

Abundance profiles constitute a major probe of the physics of the disc evolution, since they are connected to the radial dependence of several key ingredients, like star formation, infall and stellar yields, and various tracers have been explored (Luck & Lambert (2011; Magrini et al. 2017, 2023).

The abundance profiles of our model appear in Fig. 7, where they are compared to the recent data of Gaia DR3 (Gaia Collaboration et al. 2022), based on Gaia/RVS chemical data from Recio-Blanco et al. (2023). The data concern open clusters with ages <5.5 Gy found today in the Galactocentric radial range $R_G = 5-11$ kpc. Our model results are displayed for the same radial and age ranges. We notice, however, that the data do not correspond exactly to the same quantities, although sometimes such 'proxies' are used in the literature. Thus, we provide [Fe/H] values, whereas Gaia data concern [M/H] values (M referring to the average abundance of several iron-peak elements), and we use Si as proxy for the α elements[6] provided by Gaia DR3. Furthermore, our mean values are for all stars younger than 5.5 Gy found in a given radial bin, while the Gaia DR3 mean values depend obviously on the ages of the observed open clusters found in each radial bin, which are on average considerably lower than 5.5 Gy.

In the top panel of Fig. 7, the average value of the model [Fe/H] in the Solar vicinity ($R = 8$ kpc) is slightly higher than the one of the [M/H] of the observational data. Also, the slope of the metallicity profile of the model, d[Fe/H]/dR= −0.069 dex/kpc (solid curve) is slightly steeper than the data slope of d[M/H]/dR= −0.054 ± 0.008 dex/kpc (dashed curve). Both values are consistent with those recently reported in other surveys of open clusters (see

---

[6]The evolution of [Si/Fe] versus [Fe/H] is well-reproduced in the 1-zone model of the Solar neighbourhood of Prantzos et al. (2018) with the yields adopted here.

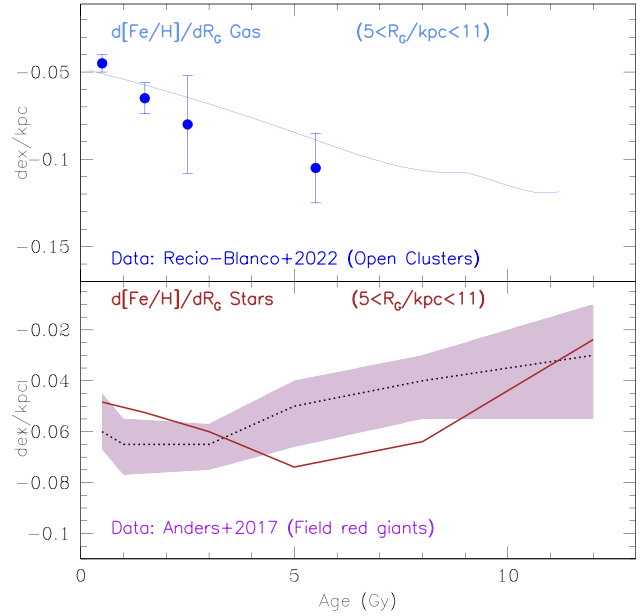**Figure 8.** Evolution of abundance gradient Δ[Fe/H]/ΔR_G (solid curves) in the range of Galactocentric radii $R_G = 5-11$ kpc, in the gas (top) and in the stars (accounting for radial migration, bottom), and comparison to observations: open clusters (top, blue dots from Gaia Collaboration et al. 2022); field red giants (bottom, dotted curve with uncertainties within the shaded aerea from Anders et al. 2017). The age bins adopted in the latter study are also used to evaluate the stellar gradient of the model.

references in Gaia Collaboration et al. 2022; Spina et al. 2022), albeit with much smaller samples. The 1σ and 2σ ranges of the model [Fe/H] values (shaded aereas) include most of the data points.

In the bottom panel of Fig. 7 are displayed the corresponding [α/Fe] ratios for the same age and radial ranges. Here, the slope of the model profile (+ 0.014 dex/kpc) is in excellent agreement with the one of the data (0.013 ± 0.007 dex/kpc), but there is an important overall offset of 0.1 dex: the model results an average value of [α/Fe]~0 in the Solar vicinity, whether Gaia DR3 data analysis suggests a value 0.1 dex lower.

At this point, we note that the profiles presented in Fig. 7 correspond to all the stars of our model, whereas Gaia DR3 data concern open clusters. It is not clear whether such massive objects are affected to the same extend as single stars by radial migration, so a direct comparison may not be appropriate. Indeed, open clusters from the inner disc, interacting strongly with inhomogeneities of the gravitational potential, may dissolve in rather short time-scales and not undergo the same amount of radial migration as field stars (Anders et al. 2017; Spina et al. 2021). Thus, despite the precision with which their ages, Galactocentric distances and chemical abundances are measured, the comparison with our model is not straightforward.

The evolution of the abundance profile has been a key issue in studies of the MW disc. Most models predict a flattening of the abundance profile of the disc gas with time, and thus a steepening of the corresponding profile of stars with age, although few ones predict the opposite effect (see Hou, Prantzos & Boissier 2000; Pilkington et al. 2012; Mollá et al. 2019, and references therein). However, the stellar abundance profile of the disc, as observed today, can be altered by radial migration, as already noticed in e.g. Minchev et al. (2013, 2014) or Kubryk, Prantzos & Athanassoula (2015b).

In the top panel of Fig. 8, we show the evolution of the [Fe/H] gradient in the gas, in the range of Galactocentric distance R_G from

5 to 11 kpc, which decreases from −0.05 dex/kpc today to −0.12 dex/kpc ∼11 Gy ago, i.e. with a rate of −0.007 dex/kpc/Gy. Blue symbols with error bars correspond the Gaia DR3 analysis of Gaia Collaboration et al. (2022) for open clusters younger than 5.5 Gy present in the same fixed range of Galactocentric radii. Despite the large error bars, the gradient clearly decreases with age, at a rate slightly larger than in our model. As emphasized before, the variation of the open cluster properties during radial migration do not allow for a straightforward comparison with our model results.

In the bottom panel of Fig. 8, we show the evolution of the [Fe/H] gradient in stars, as obervable today in the same range of Galactocentric distance R_G from 5 to 11 kpc. As already shown by Minchev et al. (2013) or Kubryk et al. (2015b), the stellar gradient is affected by radial migration and is flattened with respect to the gaseous one, because of the radial mixing of stellar populations. The effect is amplified with stellar age, since older stars have more time to migrate. This is seen in the CoRoT + APOGEE data analysed by Anders et al. (2017), showing a slight early decrease of the slope for young stars, followed by a steady increase after a few Gy.

The corresponding behaviour of our model gradient is qualitatively similar, but the decrease period lasts ∼5 Gy, taking the stellar gradient to values lower than the observed ones in that period. The subsequent rise of the gradient is also seen but it is faster than in the observations in the last age bin. In fact, the evolution of the stellar gradient in Fig. 7 (middle panel) of Kubryk et al. (2015b) is in better agreement with the data of Anders et al. (2017); the two models are similar but differ in the prescriptions of radial migration in the early Galaxy and in the stellar yields, as presented in Sections 2.1.1 and 2.1.2, respectively. At this point, we notice that in our model the gradient is evaluated by considering all the stars of a given age that are still alive today, while observations consider red giants; since the fraction of red giants in a given stellar population is a function of age and metallicity, obviously the two gradients displayed in the bottom panel of Fig. 8 are not directly comparable. More work in that respect is needed in our modelling.

As already mentioned, radial migration makes it difficult to trace back the evolution of the true abundance gradient in the gas of the disc. Based on an idea formulated in Minchev et al. (2018) and explored with numerical simulations in Lu et al. (2022b), Lu et al. (2022a) tried recently to circumvent that difficulty. They use ∼80 000 subgiant stars of LAMOST presently found in the Galactocentric distance range $R_G = 6$–12 kpc, with an average age and metallicity uncertain as small as 0.32 Gy and 0.03 dex, respectively. At each age bin they take the difference $\Delta[Fe/H] = [Fe/H]_{max} - [Fe/H]_{min}$ of the most and least metallic stars of their sample *born at the given age bin* and they assume that there exists a time-dependent linear relationship between this metallicity range and the metallicity gradient, which they normalize to the present day gradient $\Delta[Fe/H]/\Delta R$ (Age = 0) = −0.07 dex/kpc. They find a steepening of the [Fe/H] gradient with age, up to 8–11 Gy ago, at which time the trend is inversed (red squares in top panel of Fig. 9). Lu et al. (2022a) associate that feature to the last major merger (Gaia Sausage/Enceladus event) and they claim that this transition plays a major role also in shaping the [α/Fe] versus [Fe/H] dichotomy (see Section 4.3). It is interesting to note that the analysis of Lu et al. (2022a) concludes that the stars formed during that transition period have birth radii around 4–5 kpc, indicating the extend of the disc 8–11 Gy ago; indeed, the mean birth radius of the local thick disc stars in our model is around 4 kpc, as displayed in Fig. 2 (bottom panel).

Following the work of Lu et al. (2022a), we evaluate the maximum and minimum metallicity of 95 per cent of the stars currently present in the Solar neighbourhood, and the corresponding birth radii, as
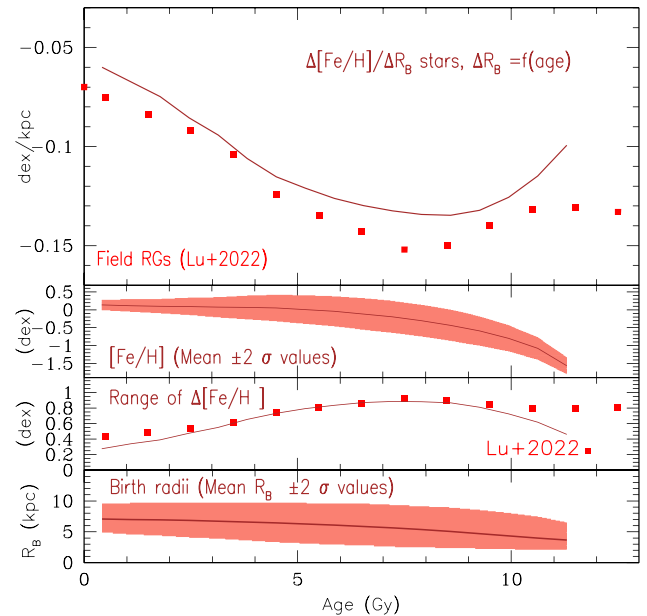

Figure 9. Top: evolution of abundance gradient $\Delta[Fe/H]/\Delta R_B$ of stars presently found in the Solar neighbourhood, evaluated from their birth radii R_B (red squares from Lu et al. 2022a) and corresponding model results (brown solid curve). Second from top: metallicities of stars presently found in Solar neighbourhood as function of their ages (mean and ±2σ values), corresponding to the middle panel of Fig. 4. Third from top: range of [Fe/H] values (in dex) used to evaluate the gradient $\Delta[Fe/H]/\Delta R_B$ in the upper panel; data (red points) from Lu et al. (2022a) and our model (brown curve). Bottom: evolution of the range of birth radii ΔR_B of stars presently found in the Solar neighbourhood (mean and 2σ values); the solid curve corresponds to the average R_B value. The ranges of $\Delta[Fe/H]$ and ΔR_B of the two bottom panels are used to evaluate the $\Delta[Fe/H]/\Delta R_B$ of the upper panel.

shown in the three lower panels of Fig. 9. The second from top panel displays the ±2σ values of metallicity (upper and lower limits of shaded aerea) around the mean (solid curve). The 3d panel from top panel displays the difference $\Delta[Fe/H] = [Fe/H]_{max} - [Fe/H]_{min}$ for each age, and we find an excellent agreement with the data points of Lu et al. (2022a). The bottom panel shows the corresponding range of birth radii ΔR_B, between the 5th and 95th percentile (shaded aerea). The abundance gradient is then obtained for each age as $\Delta[Fe/H]/\Delta R_B$. We plot our result (brown solid curve) in the top panel of Fig. 9. The gradient steepens with age in agreement with the results of Lu et al. (2022a), but it differs by 0.01–0.02 dex/kpc. We note that Lu et al. (2022a) infer the range of birth radii of their LAMOST sample by calibrating it as to get a present day gradient of −0.07 dex/kpc, which its lower than ours by ∼0.01 dex/kpc. Had they adopted a different calibration, their data points in Fig. 9 (top panel) would be found 0.01 dex/kpc higher and would then be in much better agreement with our model. Moreover, taking into account the various uncertainties involved in the observational estimate of birth radii, discussed in detail in Lu et al. (2022b), we find the agreement to be quite satisfactory.

The most important feature, however, is that the model curve also goes through a broad minimum around 9 Gy ago and then increases by 0.03 dex/kpc at the oldest ages. This change in the slope of the gradient evolution is obtained in our model because in the oldest ages the birth radii of the stars now present in the Solar neighbourhood are mostly located in the inner Galaxy: in those inner regions the abundance profile becomes flat quite early on, since they evolve on similarly short time-scales (see third panel from top panel in

Fig. 1). Outside the 4 kpc region, the gradient is quite steep early on and flattens with time. The stars that we observe locally today is a mixture of different ages and regions: old stars mostly from the inner disc (small gradient), stars of intermediate ages mostly from intermediate regions (steep gradient) and finally young stars of regions closer to the Solar neighbourhood (again smaller gradient because the abundance profile flattens with time). This evolution of the range of birth radii is displayed in the bottom panel of Fig. 9, where the average birth radius is also shown: it goes from ∼4 kpc 11 Gy ago, to ∼7 kpc at Sun's birth and ∼8 kpc today.

In summary, we find that the sample of stars locally observed is weighted in a time-dependent way that reflects the inside-out formation of the disc (more stars from the inner disc early on). In that respect, we fully agree with the conclusions of Mollá et al. (2019), namely that '*the use of a variable radial range, which takes into account the growth of the disc along the time or redshift, is an important caveat for estimating the correct evolution of the disc radial gradient.* The evolution of the stellar abundance gradient observed today results from the synergy of the aforementioned factors and goes through a minimum which corresponds to the transition, of the thick to the thin disc. However, in our case, this transition does not require some external event, as advocated in Lu et al. (2022a), but it is made 'softly' through secular evolution.

Overall, we may distinguish three types of abundance gradients:

(i) the 'true' abundance gradient in the gas, observable only today;

(ii) the abundance gradient in stars, as observed in their current Galactocentric position; its evolution is observable with sufficiently good stellar ages;

(iii) the abundance gradient that the stars currently observed in some Galactocentric position had at their birth place.

In the absence of radial migration, gradients (i) and (ii) evolve in the same way, provided that short age bins are used for (ii). Furthermore, *if* the gradients are characterized by a unique slope across the whole Galactic disc, then gradient (iii) also evolves as gradient (i). With radial migration, the evolution of gradients (i) and (ii) is different – gradient (ii) being more and more flatter for older ages –, but gradient (iii) evolves still the same as gradient (i) *in the case of a unique slope over the whole disc* at each time; this latter property was assumed and explored in the work of Lu et al. (2022a) who inferred the evolution of (i) by reconstructing first the evolution of (iii). However, if the slope of gradient (i) is not the same all over the whole disc at a given time, then radial migration makes the evolution of gradient (iii) different from both (i) and (ii); this last case was explored in this section and illustrated in Figs 8 and 9.

The properties of the Galactic disc discussed in this section, i.e. age and space distribution (resulting from the adopted scheme of inside-out disc formation and stellar radial migration through blurring and churning) affect straightforwardly the elemental abundance ratios of the corresponding stellar populations in the Solar neighbourhood, as we discuss in more detail in the next sections.

4 THE [α/FE] RATIOS IN THE THIN AND THICK DISCS

4.1 [α/Fe] versus age

Fig. 10 displays the evolution of the ratio [X/Fe] for a typical α-element, like Si. The evolution of [α/Fe] depends mostly on the history of star formation in each radial zone (upper panel). [α/Fe] decreases monotonically, because of the delayed release of Fe (about two-thirds of Solar Fe) by SNIa. The decrease is more rapid in the inner regions, where the early intense star formation produces a rapid
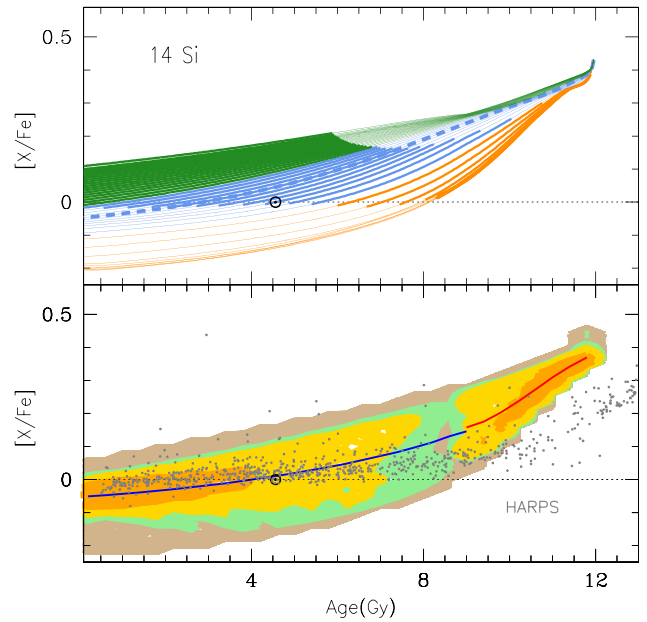

Figure 10. [Si/Fe] versus stellar age. Top: evolution of gaseous abundances in all the radial zones of the model, with colour coding as in Fig. 4. Bottom: abundances of stars present today in the thin and thick discs in the Solar cylinder (see discussion in the text); abundance data for [α/Fe] from HARPS spectra (grey points, Adibekyan et al. 2012; Delgado Mena et al. 2019).

increase of both CCSN and SNIa, and of the abundances of both Si and Fe, which reach their quasi-equilibrium values within a few Gy. In contrast, the evolution of the outer regions proceeds at much slower pace and a large fraction of their SNIa appears only at late times; as a result, their [Si/Fe] decreases slowly but steadily. The absolute value of the final [Si/Fe] ratio depends on the time integrated rates of CCSN and SNIa. The integral $\int_0^{12Gy}$ R(CCSN)/R(SNIa) dt is smaller in the inner regions than in the outer ones, and so is the corresponding final [Si/Fe] ratio: it is sub-Solar in the inner zones, but superSolar in the outer ones.

The evolution of the gas in the Solar cylinder is intermediate between the two extreme regimes, but the stars present today locally are affected in different ways: the stars born at late times (younger than the Sun) have [Si/Fe] ratios similar to those of the gas in the 7−9 kpc range, while the old stars have ratios similar to those of the gas of the early disc in the 3−4 kpc range. Thus, the change of the slope of [Si/Fe] versus age of local stars around ∼9 Gy marks indeed a transition between two regimes of star formation, but not necessarily because of a 'hiatus' in star formation, as sometimes claimed (Snaith et al. 2014): it simply reflects the fact that stars formed in different regions with different (but smooth) star formation histories and different kinematics are found today in the same location. In other terms, the adopted gradual inside-out formation of the disc provides naturally the transition between the large early slope (dominated by stars from the inner disc) and the almost flat late slope of the thin disc (dominated by local stars). This is also reflected in other chemical properties of the stars in the Solar cylinder, as we discuss in subsequent sections. But, in any case, a simple inspection of Fig. 10 suggests that, by itself, [α/Fe] cannot be considered as a reliable proxy for the age of star, although its variation is of course smaller than the one of [Fe/H], which is usually considered as such a proxy (compare the upper panels of Figs 4 and 10). Finally, as already discussed in the previous sections, the lower panel of the latter figure also shows how a 'hiatus' in the number density of stars
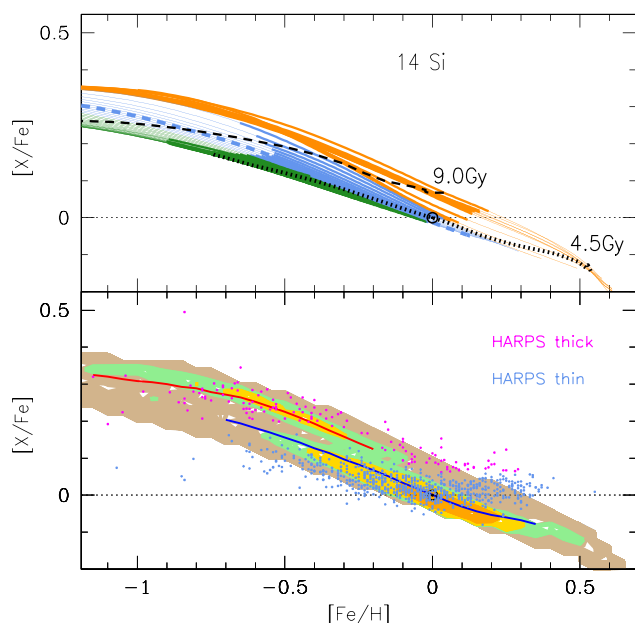
Figure 11. Same as in Fig. 4, for [Si/Fe] versus [Fe/H]. Two isochrones are displayed in the top panel, for age equal 9 Gy (dashed curve) separating the 'old' from the 'young' disc, and for age equal 4.5 Gy (dotted curve, see discussion in the text). In the bottom panel, two overdensities appear clearly through the isocontours, corresponding to those appearing in the two previous figures and representing the thick (old) and thin (young) discs. The magenta and blue points are HARPS data for [α/Fe] versus [M/H], chemically separated into thick and thin discs, respectively (Adibekyan et al. 2012).

around 8–9 Gy can be obtained without any pause in SFR or infall in any of the radial zones of the model, but simply due to the adopted inside-out scheme of disc formation.

The corresponding data in the bottom panel of Fig. 10 (grey points) from HARPS (High Accuracy Radial velocity Planet Searcher) spectra show indeed a smooth decline of [Si/Fe], but the stellar ages suffer from considerable uncertainties, preventing a meaningful comparison to the old disc of our model.

4.2 [α/Fe] versus metallicity

Fig. 11 displays the relation between [Si/Fe] versus [Fe/H], for all the zones of the model (top panel) and for the Solar cylinder (bottom panel). The isochrones in the top panel indicate snapshots at times of 3 Gy after the beginning of star formation (dashed curve, current age = 9 Gy) and 8 Gy after star formation (dotted curve, current age = 4 Gy). The former corresponds to the end of the thick disc formation, while the latter approximately to the period of Sun's formation; at that time, the metallicity in the inner zones was already $\sim 2-3$ times Solar and [Si/Fe]~ -0.1, where in the Solar vicinity ($R_G \sim 7-9$ kpc) both quantities were close to Solar.

In the bottom panel, the two sequences corresponding to the thin and thick discs are clearly separated, for the same reason as described for Figs 4, 5, and 10: the 'gap' in that region of the [Si/Fe] versus [Fe/H] diagram corresponds to a low – albeit not necessarily null – density of star formation (see top panel) and this is reflected also in the stars that populate today the Solar vicinity, after migration.

The results of the model are compared to data from HARPS spectra (Adibekyan et al. 2012; Delgado Mena et al. 2017) for the thin and thick discs. The agreement is quite satisfactory, at least for metallicities up to approximately Solar; for superSolar metallicities,

the model [Si/Fe] ratio continues to decrease with metallicity, in contrast to observations. The reason is that in the inner disc regions, late SFR is negligible and so is the production rate of alpha elements from CCSN; but SNIa, with progenitors formed in the early period of intense star formation, continue to enrich the ISM with Fe. As a result, the [α/Fe] ratio continues decreasing in the inner disc, and some of the stars formed there are found in the Solar vicinity through radial migration. It is difficult at this point to decide whether the mismatch between model and observations at the highest [Fe/H] values is due to an excessive late SNIa rate in the inner disc, or to an excessive migration of stars from that region into the Solar vicinity, caused by the adopted radial migration scheme. We note that, as shown by Santos-Peral et al. (2020) the flattening of the [α/Fe] abundance trend at superSolar metallicities could be an observational artefact due to uncertainties in the continuum placement. A specific normalization treatment as that of Santos-Peral et al. (2020) can help to recover a decreasing trend with metallicity in agreement with our model.

Finally, a comparison of the top and bottom panels of Fig. 11 shows that in our scheme the so-named High-Alpha Metal-Rich (HAMR) stars observed in the local disc can be attributed to intermediate-age stars (between 9 and 5 Gy) of the inner disc, which migrated radially to the Solar neighbourhood, as suggested already in Adibekyan et al. (2012).

4.3 Discussion on [α/Fe] versus [Fe/H] and the [Fe/H] gradient

The double sequence of [α/Fe] in the thin and thick discs of the Solar vicinity is fairly well-established by now (e.g. Adibekyan et al. 2011; Perdigon et al. 2021; Sharma et al. 2021b; Weinberg et al. 2022, and references therein) although its extent varies a lot, depending on the chosen samples and biases: number of stars, volume limit of the sample, (mixture of) elements adopted as alpha, precision of measurements, and so on. The difference in [α/Fe] for a given value of [Fe/H] between the two sequences may vary from less than 0.1 dex to more than 0.2 dex,[7] the highest metallicity of the thick-disc sequence is not well-constrained, and neither is the lowest metallicity of the thin disc.

The origin of this double sequence is not yet elucidated, and various suggestions have been made in the literature (see Section 1). In this work, we confirm, as already argued in the study of Sharma et al. (2021a) that secular evolution can produce naturally such a double sequence. In our model this results as a consequence of:

(i) inside-out disc formation, with a short time-scale for the inner disc and a longer one for the outer disc.

(ii) ratio of two elements with sources evolving on widely different time-scales: α-elements from massive stars evolving in ~ 10 Ma, versus Fe from SNIa evolving in ~ 1 Gy time-scale.

(iii) coexistence in the Solar cylinder of stars with appropriate histories of star formation, formed in the inner disc and locally.

The consequence of the above is that in the inner disc there is a large number density of stars in the [α/Fe] versus [Fe/H] plane that have large [α/Fe] values for low [Fe/H], while in the Solar neighbourhood the opposite happens. In intermediate regions, number density of stars *per unit area of the [α/Fe] versus [Fe/H] plane* is smaller, as shown in Fig. 11. Radial motions of stars through blurring and churning lead to point (iii). In summary, the adopted radial profile for the infall rate in our model (see Fig. 1, top panel), is at the origin of the gap between the thin and thick disc in the [α/Fe] versus [Fe/H] plane.

---

[7] In Section 5.1, we suggest a quantitative definition of that difference.

In their semi-analytical model, which has several different prescriptions than ours (in particular, parametrized chemical evolution) Sharma et al. (2021a) suggest a slightly different interpretation, attributing 'the gap between the two sequences to the sharp transition of [α/Fe] from a high value to a low value within a span of a few Gy, the transition being due to time delay in the on-set of SNIa explosions.'

In contrast, we note that the hybrid model of Johnson et al. (2021), adopting several ingredients similar to our model and successful in reproducing several observables of the MW disc, fails to reproduce the observed bi-modality of [α/Fe] versus [Fe/H] in the Solar neighbourhood. They suggest that a supplementary ingredient, like a two-phase star formation, would help in that respect.

At this point, we note that the recent study of Scott et al. (2021) finds, through stellar population synthesis model fitting, that the galaxy UGC 10 738 (a nearby, edge-on MW-like galaxy) contains alpha-rich and alpha-poor stellar populations with similar spatial distributions to the same components of our Galaxy. They point out that if such features are found to be generic of MW-like galaxies, this may pose a challenge for the merger-triggered starburst theory of the origin of the Milky Way's thick disc, because simulations suggest such events to be rare.

This conclusion is in contrast with the recent work of Lu et al. (2022a) who analyse ∼80 000 subgiant stars of LAMOST and find a non-monotonic of the [Fe/H] gradient – taken in the birth places of stars – around 8–11 Gy ago (see Section 3.3 and Fig. 9). They associate it to the last major merger (Gaia Sausage/Enceladus event) and they claim that this transition plays a major role in shaping the [α/Fe] versus [Fe/H] dichotomy. We show here and in Section 3.3 that this may not necessarily be the case, and that secular evolution can also reproduce both those features.

5 OTHER ELEMENTARY RATIOS

In this section, we explore the consequences of secular evolution for the ratios of other elements.

5.1 [X/Fe] ratios

The case of [α/Fe] versus [Fe/H] ratio is a clear one because of the large difference between the time-scales of massive stars and SNIa. However, the situation is less clear in other cases. From the observational point of view it is important to identify to what extent a given element X displays a simple or a double sequence (thick versus thin disc) when plotted as [X/Fe] versus [Fe/H]. For that purpose, large samples of stars with precise spectroscopically defined abundances are required.

For the present study, we adopted the AMBRE project data that is described in De Laverny et al. (2013) and consist in the automatic parametrization of large sets of ESO high-resolution archived spectra. Within the AMBRE project, the stellar atmosphere parameters (in particular, T_{eff}, log g, [Fe/H], and [X/Fe] together with their associated errors) were derived using the MATISSE algorithm (Recio-Blanco, Bijaoui & de Laverny 2006). In particular, the [X/Fe] ratios for the elements Mg, Mn, Ni, Cu, and Zn were collected from the study by Mikolaitis et al. (2017); Santos-Peral et al. (2021), those for S from Perdigon et al. (2021) and, those for Ba, Eu, and Dy from Guiglion et al. (2018). All these studies are based on HARPS and/or FEROS high resolution and high signal-to-noise spectra within the AMBRE project. This ensures that the abundances adopted here were derived in a homogeneous way using identical spectroscopic analysis tools and method (atmosphere models, spectral line lists, and spectral
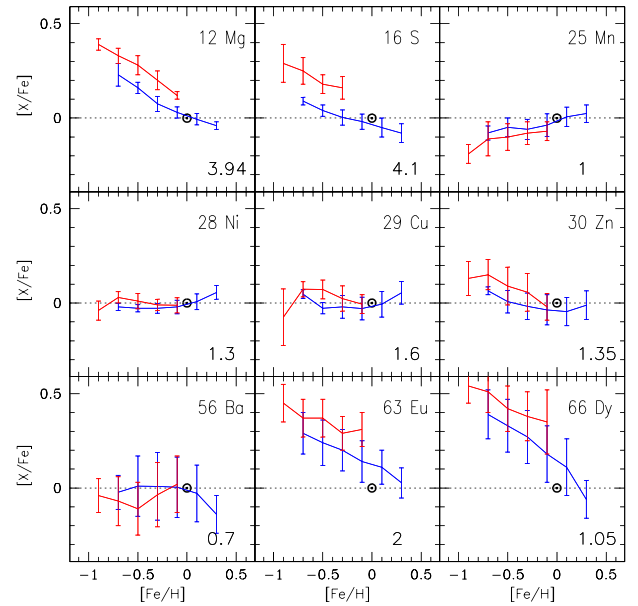

Figure 12. Observational data of [X/Fe] from the AMBRE project. Thin and thick disc stars are identified chemically (blue for thin and red for thick disc, respectively) on the basis of their [α/Fe] versus [Fe/H] behaviour (see text). Vertical bars are 1σ uncertainties and curves connect the averages of metallicity bins. The 'distance' (D) between the two sequences is expressed by the numbers on the bottom right-hand of each panel (see text for the calculation of the Z-test).

synthesis code) to derive the stellar parameters. We note that a similar analysis with the HARPS data and evaluation of the uncertainties per metallicity bin was performed by Delgado Mena et al. (2017), who also discussed some of the nucleosynthetic implications of the results. Then, we divided the selected stars according to their thin or thick disc membership following the criteria adopted by Recio-Blanco et al. (2014) based on their [α/Fe] ratio. The data for these nine elements from AMBRE analysis are displayed in Fig. 12. For each element, the chemically separated thick and thin discs are shown with red and blue colours, respectively. The common portions of the two curves are used to calculate *distances* in [X/Fe] between the thin and thick discs sequences, according to the *Z-test* (e.g. Sprinthall 2011), as follows:

At each [Fe/H] bin, the average values of [X/Fe] are determined, Y_T and Y_t for the thick and thin discs, respectively, as well as the corresponding dispersion (σ). Then, the 'distance' between the two distributions is calculated as $D = \frac{1}{N} \sum ((Y_T - Y_t)/u)$, where N is the number of [Fe/H] bins, which are common between the thin and thick disc stars (usually four), and u is given by $u = \sqrt{\sigma_T^2 + \sigma_t^2}$; σ_T and σ_t are the standard deviation of the mean ($\sigma/\sqrt{m}$) in the corresponding metallicity bin. Here $m = \min(n_T, n_t)$, where n_T and n_t are the number of stars in each metallicity bin for the thick and thin disc samples, respectively.

Values of D larger than 3 indicate that the two sequences are sufficiently distant (more than one sigma) and therefore, different. On the contrary, values of D significantly lower than 2 indicate that the two data sets cannot be distinguished. Values intermediate between 2 and 3 means that the samples are marginally different (D < 2.5), or significantly different (2.5 ≤ D < 3). These numbers are indicated in Fig. 12. Mg and S display small dispersion in all their metallicity bins and the sequences of their mean values are clearly separated, so the corresponding overall Z-distances are high (around four):
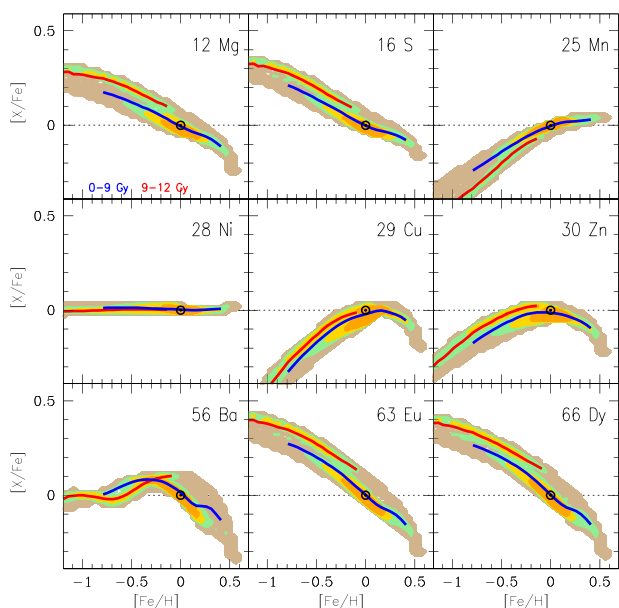
Figure 13. Model counterpart of Fig. 12. Colour coding as in Fig. 11, with the red and blue curves indicating average values for the thick and thin discs, respectively: see text for discussion of individual elements.

observationally, these two elements have clearly different [X/Fe] sequences in the local thin and thick discs. In other cases, (Mn and Ni), the sequences of mean values are very close and despite the small dispersion the corresponding Z-distances are close to 1, implying that these elements have a single sequence. For the remaining elements, low Z-distances are obtained, and this is due either to very close sequences of mean values (for Cu and Ba) or to large dispersion (for Zn and Dy). Eu appears to be a kind of intermediate case, with two clearly separated sequences (as for S), but the dispersion is rather large and leads to an intermediate value for the final Z-distance. Observationally, it is impossible with the available data to say whether Eu displays a double sequence or not.

In Fig. 13 we present our model results for the same elements. Colour-coded isocontours separate clearly the thin from thick disc sequences in the cases of some elements: alpha elements, like Mg and Si (as discussed in Section 4.2), or r-elements, like Eu and Dy. The latter is due to the fact that we adopted here, for illustration purposes, collapsars (rotating massive stars) as the sources of r-elements, with their yields scaled to the ones of oxygen (see equation 2 in Prantzos et al. 2018); the behaviour of those r-elements follows then naturally the one of oxygen in our model.

In contrast, there are cases where distinct sequences of abundance ratios [X/Fe] in the thin and thick discs do not appear. The clearest one is the case of Ni, which behaves exactly as Fe, since both of them have the same sources: they are produced in the same proportions by nuclear statistical equilibrium in the explosions of CCSN (for about 30 per cent–50 per cent of the corresponding Solar abundances) and SNIa (for the remaining 70 per cent–50 per cent).

Manganese behaves as a pseudo-secondary element in the thick disc in our model, in qualitative agreement with the observations, but with a more enhanced secondary-like behaviour than observed. This is due to the metallicity dependent yields of massive stars adopted here, which are also found in the case of the yields from Woosley & Weaver (1995) and Nomoto et al. (2013) (see discussion in Prantzos et al. 2018). Because of the strong Fe production by SNIa, the [Mn/Fe] ratio of our model flattens in the late thin disc,

in fairly good agreement with observations. It should be emphasized that the role of SNIa in the production of Mn is not yet completely understood (see discussions in Badenes, Bravo & Hughes 2008; Kobayashi, Karakas & Lugaro 2020). Our model suggests a very weak double sequence behaviour of [Mn/Fe] in the thick and early thin discs, compatible with a single sequence.

The [Cu/Fe] rises rapidly in the thick and thin discs of our model and displays a single sequence in Fig. 13. The observations of Fig. 12 show indeed a single sequence, but there is no significant rise of [Cu/Fe]. The rising of the Cu abundance of the model is due to the secondary-like nature of the dominant isotope ^{63}Cu, produced mainly by neutron captures in the He-core for metallicities higher than [Fe/H]~ -2 (see also discussion in Romano & Matteucci (2007).

In the case of Zn, our model fails to reproduce the observed trend of [Zn/Fe] > 0 in the thick disc, as well as in the halo (Prantzos et al. 2018). A supersolar ratio in the early Galaxy can be explained by invoking a considerable amount of hypernova explosions (Nomoto et al. 2013; Kobayashi et al. 2020), which we did not introduce here. It would be interesting to see whether hypernovae could produce a single or double-branch trend in the Galactic disc and whether their Zn yields depend as strongly on metallicity as the ones of massive stars adopted here. The massive star yields of Zn are mostly due to the weak s-process occurring hydrostatically in the He-core and this is the reason of their metallicity dependence, leading to a rising [Zn/Fe] at [Fe/H]< -0.5. At higher metallicities, the rising of Zn is somewhat compensated by the rising Fe from SNIa, leading to a flat profile of [Zn/Fe] with metallicity. We note that Zn is also produced in large amounts in the explosions of low-mass supernova ($\sim$8–10 M$_\odot$) through electron capture (Wanajo 2013); however, the impact of those sources is expected to be small, in view of their small number with a normal IMF.

The case of Ba is different. At low metallicities ([Fe/H] < -1) it is the r-component of Ba that matches the evolution of Fe produced by massive stars and the [Ba/Fe] ratio remains quasi-constant. Around [Fe/H]~ -1, the efficiency of the main s-process from AGB is at its maximum (Cristallo et al. 2015), but Fe production from SNIa starts becoming important and the [Ba/Fe] ratio barely increases in the late thick and early thin discs. At even higher metallicities (late thin disc), the efficiency of the main s-process is considerably reduced (Cristallo et al. 2015; Prantzos et al. 2018), while Fe production from SNIa continuous and thus the [Ba/Fe] ratio slightly decreases. The result of the operation of all these sources (AGB with metallicity dependent Ba yields and lately appearing SNIa with constant Fe yields) produce a quasi-constant [Ba/Fe] ratio over the whole history of the disc (except for the highest metallicities) and lead to a single-branch behaviour, as seen in both observations and model.

Summarizing the discussion of the models versus observations of this section we may say that for the [X/Fe] ratios in the thin and thick discs – there are cases with double sequences (Mg and S) and single ones (Ni), which are sufficiently established observationally and well understood theoretically; Mn could be also put in that class, despite some uncertainties on the role of SNIa.

(i) The large dispersion in the abundance data does not allow yet to establish the existence of a single or double sequence for Ba, Eu, or Dy observationally. Our models predict a single sequence for the s-element Ba and a double one for the r-elements Eu and Dy, but the latter result depends on the adopted assumption that r-elements are produced by collapsars (short-lived progenitors, as for the α-elements).

(ii) The observed approximately flat trend of [X/Fe] with [Fe/H] for Cu and Zn is not well-reproduced by our models, but the uncertainty on the sources/yields of those elements and their behaviour with

Table 1. Expected 1-branch (1-B) or 2-branch (2-B) behaviour of abundance ratios of elements belonging to classes A, B, C, and D (as defined below) in the local thick and thin discs.

	A: SL-MI *Mg*	B: SL-MD *Na*	C: LL-MI *Fe*	D: LL-MD *Ba*
A: SL-MI *S*	1-B, s = 0 *[S/Mg]*	1-B, s<0 *[S/Na]*	2-B, s<0 *[S/Fe]*	2-B? *[S/Ba]*
B: SL-MD *Al*	1-B, s>0 *[Al/Mg]*	1-B, s~0 *[Al/Na]*	2-B, s~0 *[Al/Fe]*	2-B? *[Al/Ba]*
C: LL-MI *Ni*	2-B, s>0 *[Ni/Mg]*	2-B, s~0 *[Ni/Na]*	2-B, s = 0 *[Ni/Fe]*	1-B *[Ni/Ba]*
D: LL-MD *La*	2-B B *[La/Mg]*	? *[La/Na]*	1-B *[La/Fe]*	1-B, s~0 *[La/Ba]*

Notes. Lifetimes of nucleosynthesis sources. SL: short lived ($\sim$10 My, CCSN); LL: long lived ($\sim$1 Gy, SNIa, AGB and perhaps NSM).
Source nucleosynthesis yields. MI: metallicity independent (primaries, even); MD: metallicity dependent (secondaries, odd).
s is the slope of the relation [X/Y] versus [Fe/H], with X on the left-hand column and Y in the top row.

metallicity leaves a lot of room for improvement. In that respect, it would help to have a clear picture of whether a single or double sequence exists for those elements. In the next subsection, we made our ideas for the importance of such sequences more explicit.

5.2 [X/Y] ratios

Trying to interpret the sequence(s) of [X/Fe] versus [Fe/H] in the previous subsection, we invoked two reasons related to the sources of the elements involved:

(i) the age of the system at the time of the enrichment of the ISM with the considered elements (because different ages allow for different types of sources to operate); and

(ii) the initial metallicity of the sources, which affects in different ways the ejected amounts of the considered elements (primaries versus secondaries or pseudo-secondaries, or odd versus even elements).

One might conceive other causes affecting the evolution of a given element, e.g. a variable IMF (either in its slope or in its upper limit), but we stick here to the simplest case of two confirmed causes; thus we distinguish – sources: short-lived (SL) versus long-lived (LL) ones; in the former case belong CCSN and collapsars (characteristic time-scales $\sim$10 Ma) and in the latter AGB stars, SNIa and NSM (time-scales 100 Ma to a few Gy) – yields: metallicity independent (MI) for primary or even elements (alpha elements, Fe, r-elements?); and metallicity dependent (MD) for secondary elements (e.g. Ba) or odd elements (e.g. Na, Al).

This scheme provides four combinations for a given element, depending on its source and nature of its yield: (i) SL-MI; (ii) SL-MD; (iii) LL-MI, and (iv) LL-MD. For the ratio of two elements we get then 16 combinations, as illustrated in Table 1. For each one of the cases (i)–(iv), two elements (X and Y) belonging to that class are selected: (S, Mg), (Al, Na), (Ni, Fe), and (La, Ba), respectively; the first one serves in the nominator and the second one in the denominator of [X/Y]. The results of our simulations for [X/Y] versus [Fe/H] appear in Fig. 14. The simplest case is obviously when both X and Y have same sources and metallicity dependence of their yields. This is illustrated by the case of [S/Mg] (primary elements produced in CCSN) and [Ni/Fe] (primaries produced first in CSSN and later also in SNIa, at the same rate). The resulting sequences are the same (one branch or 1-B) and are flat (slope = 0).

In the same case (same sources and metallicity dependence of yields) belong the couples (Al, Na) produced by CCSN and (La, Ba) made mainly by AGBs. Here, we also get a single sequence. However, the difference with the previous case is that the metallicity dependence of the yields obviously is not exactly the same for the two members of each couple. As a result, the single sequence has a slight metallicity dependence. Note that the position of the members of each couple is arbitrary: in the chosen cases, the slopes are negative, but by inverting the position of X and Y the slopes would be positive.

The next simplest case is when the two elements X and Y have the same source, but their yields have substantially different metallicity dependence (MD), like a primary versus a secondary (or an odd) element. Then a single sequence is also obtained, because of the same time-scale of the evolution of sources, but it has a strong slope, either negative (when the MD element is in the denominator, like [S/Na]) or positive (when the MD element is in the nominator, as in the case of [Al/Mg]).

The next case is the one most extensively analysed, namely two primary elements with sources evolving on different time-scales (SL and LL). This is typically the case of [α/Fe] ratio, discussed in Section 4.2. It leads to 2 quasi-parallel branches (2-B), as illustrated here for [S/Fe]: its slope is negative because the LL element (Fe) is in the denominator. The 'mirror'-case is [Ni/Mg], with two sequences and a positive slope, since the LL element (Ni) is in the nominator.

The previous cases involve elements having at least one common feature, either source lifetime or yield metallicity dependence, or both. The situation becomes more complicated when the two elements have no common feature. It is well-known that the effects of metallicity dependence of the yields may mimic to some extent those of a source with long lifetime.

Those effects are illustrated in the case of [Al/Fe]. Al is a SL-MD element (see Table 1), while Fe is a LL-MI. In Fig. 14, a 2-branch behaviour appears for the thin and thick discs, due to the difference in source lifetimes. On the other hand, the metallicity dependence of Al yields from CCSN compensates somewhat for the late production of Fe in SNIa and leads to a rather flat curve in the late thick disc and in the thin disc. The behaviour of [Ni/Na] is the mirror image of that, since the SL-MD element (Na) is now in the denominator.

The s-elements Ba and La are displayed here only for illustration purposes, since their case is even more complex than the previous ones. They start with an r-component the importance of which is reduced at later times, because of the rising s-component from the main s-process in LL AGBs. This matches to some extent the rising contribution of Fe-peak elements from SNIa and, along with the long lifetime of AGBs, contribute to produce a single branch behaviour. In the superSolar metallicity regime of the thin disc, the efficiency of the s-process is reduced and the ratio of those s-elements to Fe declines. These results are illustrated in the behaviour of [La/Fe] and its mirror image of [Ni/Ba].

Although our results on [La/Mg] and [La/Na] (as well as their mirror images of [S/Ba] and [Al/Ba]) seem to suggest a 2-branch behaviour, we refrain from any conclusions, since the corresponding overdensities in the [X/Fe] versus [Fe/H] plane for the early thin disc are fairly weak.

Finally, in the cases of [La/Fe] and [Ni/Ba], we observe that the late increase of the SNIa products (Fe and Ni), combined with the decrease of the efficiency of main s-process production (for Ba and La) at high metallicity, leads to a decrease of [La/Fe] and a corresponding increase of [Ni/Ba] for [Fe/H] > 0. This result depends on both the adopted AGB yields at high metallicity and the rate of SNIa in the inner disc regions, where the superSolar metallicity stars are assumed to be formed.
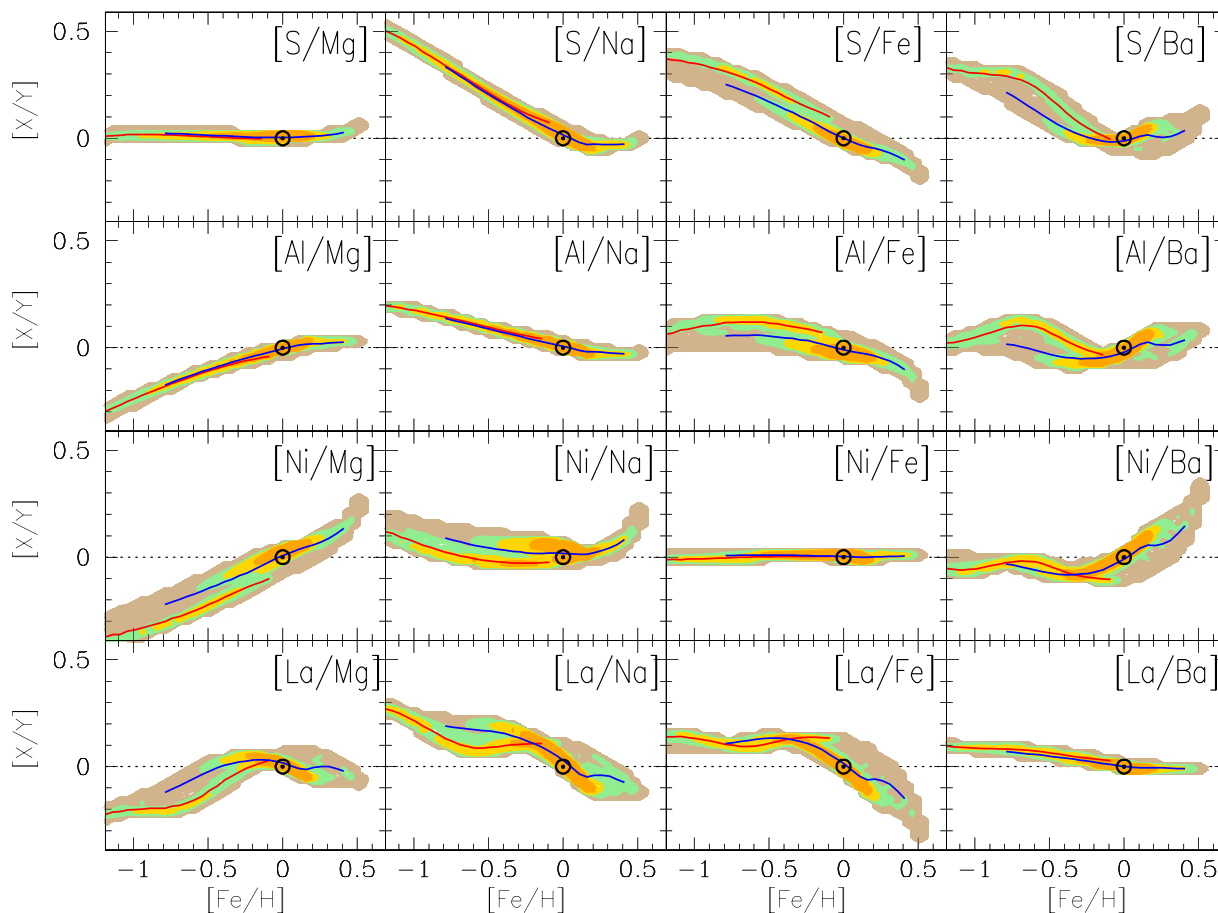
Figure 14. Model results for the Solar cylinder and for [X/Y] abundance ratios versus [Fe/H], for couples of elements X and Y arranged as in Table 1.

We remind that in the simulation studied here we assumed, for illustration purposes, production of the r-component of all heavy elements in collapsars evolving on short time-scales. Those elements behave then obviously as alpha elements in our calculations, as already shown in Fig. 13 for Eu and Dy. However, since the source(s) of those elements still remain uncertain and they may evolve on a range a time-scales, we prefer to post-pone a more thorough discussion of that topic for a future paper.

It is interesting to notice that whenever a '2-branch' behaviour is obtained in our scheme, the two branches are reversed in the 'mirror image': if the [X/Y] sequence of the thick disc is higher than the one of the thin disc for a given metallicity, it appears below it in the mirror image, as e.g. in the cases of [Ni/Mg] versus [Si/Fe] or [Ni/Na] versus [Al/Fe].

The results displayed in Fig. 14 and discussed in the previous paragraphs concern the local disc, and more precisely, the Solar cylinder (a region of width of $\Delta R \sim 1$ kpc center at Galactocentric distance of ~ 8 kpc). Results are different for other disc regions, as illustrated in Figs 15 and 16.

In Fig. 15, we show the results for the region 2–3.5 kpc. In this case the duality is very strongly diminished, so that one could say that there is a single sequence (albeit with a finite width) for all element ratios. The reason is obviously that those inner regions evolved on similarly short time-scales, and thus have a common evolution, while they received little contribution from the outer disc, which evolved on long time-scales. A comparison with Fig. 14 reveals two more features. First, at subSolar metallicities, the unique sequence of Fig. 15 corresponds to the thick-disc sequence of the
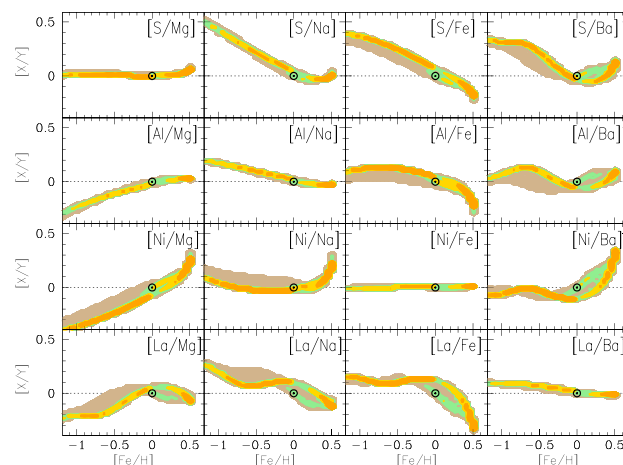

Figure 15. Same as in Fig. 14, but this time for the inner disc, in the radial range of 2–3.5 kpc.

local disc (the red-coloured sequence in Fig. 14). This is a clear signature that the local thick disc has a common origin with the inner disc. Secondly, there is an overdensity of stars at superSolar metallicities [Fe/H]$\sim +0.3 - +0.5$ dex, which corresponds to the late saturation of metallicity in the inner disc (see the two bottom panels of Fig. 1). Such an overdensity does not exist in the local disc, but clearly its superSolar metallicity stars come from those
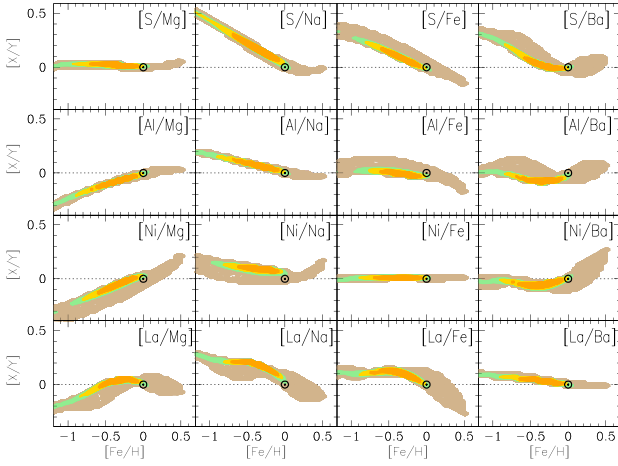
Figure 16. Same as in Fig. 14, but this time for the outer disc, in the radial range of 12–15 kpc.

inner disc regions through radial migration, as discussed in Section 3.2.

In Fig. 16, we display the same results for the outer disc, in the region 12–14 kpc. Again, no double sequence is obtained for any element ratio. Those regions evolve on similarly long timescales and receive very little contribution from the inner disc through radial migration, thus they display again a single sequence in their elementary abundance ratios. In contrast to the previous case of the inner disc, this single sequence is close to the thin disc sequence of the Solar cylinder (the blue curves in Fig. 14). Furthermore, there are basically no superSolar metallicity stars in those outer disc regions; very few of the large numbers of such stars formed in the inner disc manage to reach the outer disc through radial migration, since the required time to cross ~10 kpc is ~10 Gy.

We note that a direct comparison of our results with observations is not always feasible, since our model is a 1D and provides results for a given Galactocentric radius, but not as a function of distance from the plane. On the other hand, because of dust extinction in the Galactic plane, existing observations provide results for the inner and outer discs mostly at high galactic latitudes, which are representative essentially of the thick disc. For instance Lian et al. (2020) select ~40 000 stars from Sloan Digital Sky Survey (SDSS) DR16 with high signal to noise ratio and chose to define the thick disc geometrically, as stars at distances d >1 kpc from the mid-plane of the Galactic disc. When the ensemble of all stars in the region $4 < R$ (kpc) <8 is considered (left-hand panel in their Fig. 2), two overdensities appear in the [α/Fe] versus [Fe/H] diagram, in the top left (high [α/Fe], low [Fe/H]) and bottom right (low [α/Fe] and superSolar [Fe/H]). Both those features appear also in our Fig. 15 for the inner disc. They are due to the fact that at late times the abundances of most zones in the inner disc reach a 'saturation equilibrium', where the metals produced by the few stars newly formed are diluted by the metal-poor gas ejected by the numerous stars formed in these zones during the early times; for that reason, the number density of stars is high in that region of the [α/Fe] versus [Fe/H] plane.

5.3 Discussion on [X/Y] ratios

In the previous section, we attempted a classification of the various abundance patterns that are expected to arise in the thin and thick discs of the Galaxy, on the basis of the properties of the corresponding nucleosynthesis sources and yields. Indeed, in view of the large

number of existing and forthcoming data, some classification scheme is required for the expectations to be compared to observations. We discuss here two recent attempts in that direction.

Weinberg et al. (2019) used ~20 000 stars of the upper red giant branch from APOGEE DR14 survey to map the trends of elemental abundance ratios across the Galactic disc, spanning the radial range $R = 3-15$ kpc and mid-plane distance $|z| = 0-2$ kpc for 15 elements: O, Na, Mg, Al, Si, P, S, K, Ca, V, Cr, Mn, Co, and Ni. In view of the uncertainties on Fe production and evolution (due to mass cut and explosion energy in SNII, or to the uncertain evolution of the rate of SNIa), instead of using Fe as a reference element (i.e. [Fe/H] as a proxy for time) they chose Mg, which is well-measured by APOGEE and is solely produced by CCSN.[8] Separating the stars in two populations according to their [Fe/Mg] ratio, the work of Weinberg et al. (2019) revealed that the median trends in the [X/Mg] versus [Mg/H] plane in each population are almost independent of location in the Galaxy, and that the observed trends can be explained with a semi-empirical 'two-process' model that describes both the ratio of CCSN and Type Ia contributions to each element and the possible metallicity dependence of the supernova yields. They conclude that these observationally inferred trends can provide strong tests of supernova nucleosynthesis calculations, at least in the simple framework they consider (i.e. neglecting variations of the IMF or the CCSN range with time or metallicity). They do not attempt, however, to characterize those observed patterns in terms of the existence of single or double abundance sequences.

More recently, Sharma et al. (2022) studied the dependence of elemental abundances on stellar age and metallicity among a sample of about 50 000 main-sequence turn off (MSTO) and ~3700 giants Galactic disc stars from the GALAH DR3 survey (Buder et al. 2021). Ages and distances of the stars were computed from observed parameters by making use of stellar isochrones and parallax in the case of MSTO stars, or asteroseismic observables in the case of giant stars (see Sharma et al. 2018, for details). These authors found that elemental abundances for 23 elements show trends with both age and metallicity. They studied the relation between the variation of [X/Fe] with metallicity and age separately. The relation and the relationship is well-described by a simple model in which the dependence of the [X/Fe] ratio on age and [Fe/H] are additively separable. Then, elements can be grouped in the age–[Fe/H] plane and the different groups can be associated with different nucleosynthetic sites: massive stars, exploding white dwarfs, and AGB stars. Since the stars studied cover a large range in Galactocentric ($R, |z|$) locations, and the trends found are similar to both MSTO and giant stars, the authors suggested that their results may be valid over the whole disc of the Galaxy. This result may have significant implications for Galactic archaeology since it makes possible to estimate the age and birth radius of the stars using abundances, and from this dynamical processes like radial migration and star formation histories at different radial zones can be explored.

The project of Sharma et al. (2022) is attractive, because it is based on simple assumptions: the composition of a star is uniquely characterized by its formation time and radial position and that the interstellar medium is fully homogeneous (chemically) at any time in a given place. This may indeed apply, at least to a first order, as discussed in Sharma et al. (2022) and suggested by observational arguments and semi-analytical models, which show that the trajectories of various radial zones in the planes of age–

---

[8]For similar reasons, Goswami & Prantzos (2000) suggested to replace Fe by an alpha-element like O or Ca (see their section 5.7 and Fig. 8).

metallicity or [X/Fe]–metallicity are monotonic and do not mix with each other (e.g. Schönrich & Binney 2009; Kubryk et al. 2015a; Johnson et al. 2021; Sharma et al. 2021a, and this work). However, it may not apply in cases where the star formation did not evolve smoothly, e.g. through episodes of intense star formation like those recently reported for the Galactic disc (Mor et al. 2019; Ruiz-Lara et al. 2020; Sahlholdt, Feltzing & Feuillet 2022): depending on their intensity and spatial extension, such episodes may lead to a mixing of the aforementioned trajectories and to degeneracy in determining the time and place of birth of a star from its composition. Similar effects – albeit less important – could result from localized intense episodes of infall.

Independently of the aforementioned complications, Sharma et al. (2022) use the slopes of the observed [X/Fe] versus age or metallicity relations for rather large ranges of those parameters (3–11 Gy for ages and −0.6–0.2 in [Fe/H]). The derived unique slopes are then used to group the various elements X in the plane of Δ[X/Fe]/Δ[Fe/H] versus Δ[X/Fe]/Δ(log(Age). However, the large ranges of the adopted parameters may mask important variations of the adopted slopes and lead to spurious results in the classification of the elements in that plane. For instance, an inspection of fig. 9 in Sharma et al. (2022) shows that Na appears to be the element with the closest behaviour to Fe, much closer than Ni, while on the other hand Ba and La appear to behave in quite different ways, although they both belong to the second peak of the s-process.

Our approach is less ambitious than the one of either Weinberg et al. (2019) or Sharma et al. (2022), because it does not aim to provide a quantitative classification of the elements in terms of their nucleosynthetic origin, but only a qualitative one: the existence of one or two branches in [X/Fe] (or [X/Y]) versus [Fe/H] relation.

6 SUMMARY AND CONCLUSIONS

In this study, we present an updated version of the 1D semi-analytical model of Kubryk et al. (2015a, b), describing the evolution of the Milky way disc. The model includes a parametrized treatment of radial migration inspired by *N*-body + SPH simulations, which accounts both for 'passive tracers' of chemical evolution and 'active long-lived agents' of nucleosynthesis (like SNIa and AGB stars).

The model reproduces fairly well several observed features of the present day MW disc, like the recently observed gradients of [Fe/H] and [α/Fe] from Open Clusters (Gaia Collaboration et al. 2022, Gaia-DR3 results) or the up-turn in the local age-metallicity relation for superSolar metallicity stars, anticipated in Kubryk et al. (2015a) and observed by Feuillet et al. (2018, 2019), which it believed to constitute a clear signature of radial migration in the thin disc (see Section 3).

A key feature of the model is the formation of the thick disc by secular evolution. In our case this occurs as a consequence of (Section 4):

(i) inside-out disc formation, with a short time-scale for the inner disc and a longer one for the outer disc.

(ii) ratio of two elements with sources evolving on widely different time-scales: α-elements from massive stars evolving in $\sim$ 10 My, versus Fe from SNIa evolving in $\sim$1 Gy time-scale.

(iii) coexistence in the Solar cylinder of stars with appropriate histories of star formation, the thick disc being made from stars formed early on in the rapidly evolved inner disc.

This scenario for the formation of the thick disc can explain its chemical properties, like the long established double-branch behaviour of [α/Fe] versus [Fe/H] in the Solar neighbourhood. It can also explain the recently evaluated non-monotonic evolution with

age of the metallicity gradient, as inferred by Lu et al. (2022a) for the birth radii of stars currently present in the Solar neighbourhood: after a steady decrease, the gradient becomes flatter at the oldest ages, a behaviour remotely reminiscent of the one concerning not the birth radii, but the current Galactocentric radii of stars. In contrast to Lu et al. (2022a) who favour early mergers as an explanation of that behaviour, we argue here that it may result from a combination of radial migration *and* a variable (non-unique) slope of the abundance profiles across the Galactic discs (Section 3.3).

However, these successes do not imply that secular evolution was the only factor shaping the thick and thin discs. The high velocity dispersion of old stars can be attributed to an early highly turbulent phase – as assumed here – but also to early mergers, as advocated in various studies (see Section 1 for references). Our scenario, in line with e.g. Schönrich & Binney (2009), Loebman et al. (2011), Hayden et al. (2017), and Sharma et al. (2021a, 2022), does not require some particular event (a merger, or the paucity of star formation on Gy time-scales and/or intense episodes of infall) to explain the chemical properties of the thick disc.

In Section 5, we explore the consequences of our model for other abundance ratios [X/Y] in the MW disc. We suggest that a key parameter in such studies is the 'abundance distance' separating the thick from the thin disc sequences of [X/Y]. We illustrate that suggestion by adopting a simple $Z-$test to measure that distance in the case of a set of high resolution observations analysed in the AMBRE project (De Laverny et al. 2013) for a handful of elements (Mg, S, Mn, Ni Cu, Zn, Ba, Eu, and Dy). We show that, barring observational uncertainties, that technique has a high diagnostic potential, since it separates clearly elements with sources evolving on different time-scales, like e.g. α-elements from Fe. In that respect, it would be interesting to have a precise evaluation of the abundance distance between the thin and thick discs for r-elements, their main source being poorly known at present. If collapsars are the main source, then a double branch would be expected, as displayed in Fig. 12 for [Eu/Fe]; in contrast, if the main source is neutron star mergers, the thick and thin disc branches would be expected to be very close.

Finally, we generalize that method to the ratios of any two elements X and Y, with nucleosynthesis sources differing either in one or both of their two key properties, namely time-scale of their evolution and metallicity dependence of their yields. We find that it is the time-scale difference that plays always the key role in producing distinct [X/Y] sequences for the thin and the thick discs, while the metallicity dependence of the corresponding yields plays rather a minor role.

We emphasize that the above conclusions/predictions are obtained within the adopted framework of the formation of the thick disc. Other modes of thick disc formation, e.g. through the action of early galaxy mergers, may lead to different chemical signatures and should be investigated as well.

DATA AVAILABILITY

Data sets generated during the current study are available from the corresponding author on reasonable request.

REFERENCES

Abdurro'uf et al., 2022, ApJS, 259, 35

Adibekyan V. Z., Santos N. C., Sousa S. G., Israelian G., 2011, A&A, 535, L11

Adibekyan V. Z., Sousa S. G., Santos N. C., Delgado Mena E., González Hernández J. I., Israelian G., Mayor M., Khachatryan G., 2012, A&A, 545, A32

Agertz O., Teyssier R., Moore B., 2009, MNRAS, 397, L64

Agertz O. et al., 2021, MNRAS, 503, 5826

Anders F. et al., 2017, A&A, 600, A70

Anguiano B. et al., 2020, AJ, 160, 43

Athanassoula E., Rodionov S. A., Peschken N., Lambert J. C., 2016, ApJ, 821, 90

Aumer M., Binney J., Schönrich R., 2016, MNRAS, 462, 1697

Badenes C., Bravo E., Hughes J. P., 2008, ApJ, 680, L33

Bekki K., Tsujimoto T., 2011, ApJ, 738, 4

Belokurov V., Kravtsov A., 2022, MNRAS, 514, 689

Bensby T., Feltzing S., Lundström I., Ilyin I., 2005, A&A, 433, 185

Bensby T., Feltzing S., Oey M. S., 2014, A&A, 562, A71

Beraldo e Silva L., Debattista V. P., Nidever D., Amarante J. A. S., Garver B., 2021, MNRAS, 502, 260

Binney J., Sanders J. L., 2014, in Feltzing S., Zhao G., Walton N. A., Whitelock P.eds, Vol. 298, Setting the scene for Gaia and LAMOST. Cambridge Univ. Press, Cambridge, p. 117

Bird J. C., Kazantzidis S., Weinberg D. H., Guedes J., Callegari S., Mayer L., Madau P., 2013, ApJ, 773, 43

Bland-Hawthorn J., Gerhard O., 2016, ARA&A, 54, 529

Blitz L., Rosolowsky E., 2006, ApJ, 650, 933

Bournaud F., Elmegreen B. G., Martig M., 2009, ApJ, 707, L1

Bovy J., Rix H.-W., Liu C., Hogg D. W., Beers T. C., Lee Y. S., 2012, ApJ, 753, 148

Brook C. B. et al., 2012, MNRAS, 426, 690

Brucy N., Hennebelle P., Bournaud F., Colling C., 2020, ApJ, 896, L34

Buck T., 2020, MNRAS, 491, 5435

Buder S. et al., 2021, MNRAS, 506, 150

Burkert A., Truran J. W., Hensler G., 1992, ApJ, 391, 651

Cartledge S. I. B., Lauroesch J. T., Meyer D. M., Sofia U. J., 2006, ApJ, 641, 327

Chiappini C., 2009, in Andersen J., Nordström B., Bland-Hawthorn J.eds, Vol. 254, The Galaxy Disk in Cosmological Context. Cambridge Univ. Press, Cambridge, p. 191,

Chiappini C., Matteucci F., Gratton R., 1997, ApJ, 477, 765

Ciucǎ I. et al., 2023, MNRAS, doi:10.1093/mnrasl/slad033

Conroy C. et al., 2022, preprint (arXiv:2204.02989)

Cristallo S., Straniero O., Piersanti L., Gobrecht D., 2015, ApJS, 219, 40

Dantas M. L. L. et al., 2022, A&A, 669, 17

De Laverny P., Recio-Blanco A., Worley C. C., De Pascale M., Hill V., Bijaoui A., 2013, The Messenger, 153, 18

Delgado Mena E., Tsantaki M., Adibekyan V. Z., Sousa S. G., Santos N. C., González Hernández J. I., Israelian G., 2017, A&A, 606, A94

Delgado Mena E. et al., 2019, A&A, 624, A78

Everall A., Belokurov V., Evans N. W., Boubert D., Grand R. J. J., 2022, MNRAS, 511, 3863

Feltzing S., Bowers J. B., Agertz O., 2020, MNRAS, 493, 1419

Feuillet D. K. et al., 2018, MNRAS, 477, 2326

Feuillet D. K., Frankel N., Lind K., Frinchaboy P. M., García-Hernández D. A., Lane R. R., Nitschelm C., Roman-Lopes A., 2019, MNRAS, 489, 1742

Forbes J., Krumholz M., Burkert A., 2012, ApJ, 754, 48

Frankel N., Rix H.-W., Ting Y.-S., Ness M., Hogg D. W., 2018, ApJ, 865, 96

Fuhrmann K., 1998, A&A, 338, 161

Gaia Collaboration et al., 2023, A&A, in press, doi:10.48550/arXiv.2206.05534

Gaia Collaboration et al., 2022, preprint (arXiv:2206.05534)

Gent M. R., Eitner P., Laporte C. F. P., Serenelli A., Koposov S. E., Bergemann M., 2022, preprint (arXiv:2206.10949)

Gilmore G., Reid N., 1983, MNRAS, 202, 1025

Goswami A., Prantzos N., 2000, A&A, 359, 191

Grand R. J. J. et al., 2018, MNRAS, 474, 3629

Grand R. J. J. et al., 2020, MNRAS, 497, 1603

Grisoni V., Spitoni E., Matteucci F., Recio-Blanco A., de Laverny P., Hayden M., Mikolaitis Ŝ., Worley C. C., 2017, MNRAS, 472, 3637

Guiglion G., de Laverny P., Recio-Blanco A., Prantzos N., 2018, A&A, 619, A143

Hayden M. R., Recio-Blanco A., de Laverny P., Mikolaitis S., Worley C. C., 2017, A&A, 608, L1

Haywood M., 2008, MNRAS, 388, 1175

Helmi A., 2020, ARA&A, 58, 205

Hou J. L., Prantzos N., Boissier S., 2000, A&A, 362, 921

Iwamoto K., Brachwitz F., Nomoto K., Kishimoto N., Umeda H., Hix W. R., Thielemann F.-K., 1999, ApJS, 125, 439

Jeffreson S. M. R., Keller B. W., Winter A. J., Chevance M., Kruijssen J. M. D., Krumholz M. R., Fujimoto Y., 2021, MNRAS, 505, 1678

Johnson J. W. et al., 2021, MNRAS, 508, 4484

Karakas A. I., 2010, MNRAS, 403, 1413

Kawata D., Chiappini C., 2016, Astronomische Nachrichten, 337, 976

Khoperskov S., Haywood M., Snaith O., Di Matteo P., Lehnert M., Vasiliev E., Naroenkov S., Berczik P., 2021, MNRAS, 501, 5176

Kobayashi C., Karakas A. I., Lugaro M., 2020, ApJ, 900, 179

Kroupa P., 2002a, Science, 295, 82

Kroupa P., 2002b, MNRAS, 330, 707

Kubryk M., Prantzos N., Athanassoula E., 2013, MNRAS, 436, 1479

Kubryk M., Prantzos N., Athanassoula E., 2015a, A&A, 580, A126

Kubryk M., Prantzos N., Athanassoula E., 2015b, A&A, 580, A127

Li Y., Mo H. J., van den Bosch F. C., Lin W. P., 2007, MNRAS, 379, 689

Li Z., Zhao G., Chen Y., Liang X., Zhao J., 2022, MNRAS, 517, 4875L

Lian J. et al., 2020, MNRAS, 497, 2371

Limongi M., Chieffi A., 2018, ApJS, 237, 13

Loebman S. R., Roškar R., Debattista V. P., Ivezić Ž., Quinn T. R., Wadsley J., 2011, ApJ, 737, 8

Lu Y., Minchev I., Buck T., Khoperskov S., Steinmetz M., Libeskind N., Cescutti G., Freeman K. C., 2022a, Nature, preprint (arXiv:2212.04515)

Lu Y., Buck T., Minchev I., LuNess M. K., 2022b, MNRAS, 515, L34

Luck R. E., Lambert D. L., 2011, AJ, 142, 136

Mackereth J. T. et al., 2019, MNRAS, 489, 176

Magrini L. et al., 2017, A&A, 603, A2

Magrini L. et al., 2023, A&A, 669, A119

Maoz D., Graur O., 2017, ApJ, 848, 25

Miglio A. et al., 2021, A&A, 645, A85

Mikolaitis Š., de Laverny P., Recio-Blanco A., Hill V., Worley C. C., de Pascale M., 2017, A&A, 600, A22

Minchev I., 2016, Astronomische Nachrichten, 337, 703

Minchev I., Famaey B., Quillen A. C., Dehnen W., Martig M., Siebert A., 2012, A&A, 548, A127

Minchev I., Chiappini C., Martig M., 2013, A&A, 558, A9

Minchev I., Chiappini C., Martig M., 2014, A&A, 572, A92

Minchev I. et al., 2018, MNRAS, 481, 1645

Minniti J. H. et al., 2020, A&A, 640, A92

Mollá M., Díaz Á. I., Cavichia O., Gibson B. K., Maciel W. J., Costa R. D. D., Ascasibar Y., Few C. G., 2019, MNRAS, 482, 3071

Mor R., Robin A. C., Figueras F., Roca-Fàbrega S., Luri X., 2019, A&A, 624, L1

Navarro J. F., Abadi M. G., Venn K. A., Freeman K. C., Anguiano B., 2011, MNRAS, 412, 1203

Nieva M. F., Przybilla N., 2012, A&A, 539, A143

Noguchi M., 2018, Nature, 559, 585

Nomoto K., Kobayashi C., Tominaga N., 2013, ARA&A, 51, 457

Park M. J. et al., 2021, ApJS, 254, 2

Perdigon J., de Laverny P., Recio-Blanco A., Fernandez-Alvar E., Santos-Peral P., Kordopatis G., Álvarez M. A., 2021, A&A, 647, A162

Philcox O., Rybizki J., Gutcke T. A., 2018, ApJ, 861, 40

Pilkington K. et al., 2012, A&A, 540, A56

Prantzos N., Abia C., Limongi M., Chieffi A., Cristallo S., 2018, MNRAS, 476, 3432

Prantzos N., Abia C., Cristallo S., Limongi M., Chieffi A., 2020, MNRAS, 491, 1832

Quinn P. J., Hernquist L., Fullagar D. P., 1993, ApJ, 403, 74

Randich S. et al., 2022, A&A, 666, A121

Recio-Blanco A., Bijaoui A., de Laverny P., 2006, MNRAS, 370, 141

Recio-Blanco A. et al., 2014, A&A, 567, A5

Recio-Blanco A. et al., 2023, A&A, in press

Renaud F., Agertz O., Read J. I., Ryde N., Andersson E. P., Bensby T., Rey M. P., Feuillet D. K., 2021, MNRAS, 503, 5846

Rix H.-W., Bovy J., 2013, A&A Rev., 21, 61

Romano D., Matteucci F., 2007, MNRAS, 378, L59

Roškar R., Debattista V. P., Quinn T. R., Stinson G. S., Wadsley J., 2008, ApJ, 684, L79

Ruiz-Lara T., Gallart C., Bernard E. J., Cassisi S., 2020, Nat. Astron., 4, 965

Sahlholdt C. L., Feltzing S., Feuillet D. K., 2022, MNRAS, 510, 4669

Sanders J. L., Binney J., 2015, MNRAS, 449, 3479

Santos-Peral P., Recio-Blanco A., de Laverny P., Fernández-Alvar E., Ordenovic C., 2020, A&A, 639, A140

Santos-Peral P., Recio-Blanco A., Kordopatis G., Fernández-Alvar E., de Laverny P., 2021, A&A, 653, A85

Schönrich R., Binney J., 2009, MNRAS, 396, 203

Scott N., van de Sande J., Sharma S., Bland-Hawthorn J., Freeman K., Gerhard O., Hayden M. R., McDermid R., 2021, ApJ, 913, L11

Sellwood J., Binney J., 2002, MNRAS, 336, 785

Sharma S. et al., 2018, MNRAS, 473, 2004

Sharma S. et al., 2021a, MNRAS, 506, 1761

Sharma S., Hayden M. R., Bland-Hawthorn J., 2021b, MNRAS, 507, 5882

Sharma S. et al., 2022, MNRAS, 510, 734

Snaith O. N., Haywood M., Di Matteo P., Lehnert M. D., Combes F., Katz D., Gómez A., 2014, ApJ, 781, L31

Spina L. et al., 2021, MNRAS, 503, 3279

Spina L., Magrini L., Cunha K., 2022, Universe, 8, 87

Spitoni E. et al., 2021, A&A, 647, A73

Sprinthall R., 2011, in Basic Statistical Analysis. 9th edn. Pearson, London, p. 672

Steinmetz M. et al., 2020, AJ, 160, 83

Vieira K., Carraro G., Korchagin V., Lutsenko A., Girard T. M., van Altena W., 2022, ApJ, 932, 28

Villalobos Á., Helmi A., 2008, MNRAS, 391, 1806

Vincenzo F., Kobayashi C., 2020, MNRAS, 496, 80

Vincenzo F., Weinberg D. H., Miglio A., Lane R. R., Roman-Lopes A., 2021, MNRAS, 508, 5903

Wanajo S., 2013, ApJ, 770, L22

Wanajo S., Hirai Y., Prantzos N., 2021, MNRAS, 505, 5862

Weinberg D. H. et al., 2019, ApJ, 874, 102

Weinberg D. H. et al., 2022, ApJS, 260, 32

Wilson M. L. et al., 2011, MNRAS, 413, 2235

Woosley S. E., Weaver T. A., 1995, ApJS, 101, 181

Xiang M., Rix H.-W., 2022, Nature, 603, 599

Yan Y., Du C., Liu S., Li H., Shi J., Chen Y., Ma J., Wu Z., 2019, ApJ, 880, 36

This paper has been typeset from a TEX/LATEX file prepared by the author.